Received August 27, 2020; accepted September 28, 2020. Date of publication 1 October 2020; date of current version 22 October 2020.

Digital Object Identifier 10.1109/OJAP.2020.3028220

Millimeter-Wave Power Harvesting: A Review

MAHMOUD WAGIH (Graduate Student Member, IEEE), ALEX S. WEDDELL (Member, IEEE), AND STEVE BEEBY (Senior Member, IEEE)

School of Electronics and Computer Science, University of Southampton, Southampton SO17 1BJ, U.K.

CORRESPONDING AUTHOR: M. WAGIH (e-mail: mahm1g15@ecs.soton.ac.uk)

This work was supported in part by the European Commission through the Project EnABLES: European Infrastructure Powering the Internet of Things, funded through H2020-EU.1.4.1.2 under Grant 730957, and in part by the U.K. Engineering and Physical Sciences Research Council under Grant EP/P010164/1.

ABSTRACT The broad spectrum available at millimeter-wave (mmWave) bands has attracted significant interest for a breadth of applications, with 5G communications being the main commercial drive for mmWave networks. Wireless power transmission and harvesting at mmWave bands have attracted significant attention due to the potential for minimizing the harvesting antenna size, allowing for more compact rectennas. For a fixed antenna size, the received power increases with frequency. Nevertheless, several challenges lie in realizing high efficiency antennas and rectifiers at mmWave bands. This article reviews the recent advances in mmWave rectenna design at a component- and system-level. Low-cost antennas and components for mmWave power harvesting, such as high efficiency scalable rectifiers on polymers and high radiation efficiency antennas on textiles, are reviewed. Both the antenna and rectifier can be realized using low-cost fabrication methods such as additively-manufactured circuits and packages, in addition to digital integrated circuits (ICs) for the rectifiers. Finally, this article provides an overview of future antenna design challenges and research directions for mmWave power harvesting.

INDEX TERMS Antennas, Internet of Things, microstrip antennas, millimeter-wave antennas, rectennas, rectifiers, RF energy harvesting, wireless power transfer.

I. INTRODUCTION

POWER-AUTONOMY is seen as a key requirement of future Internet of Things (IoT) networks [1]. As semiconductor devices have scaled to mm and sub-mm dimensions, there is a desire for compact yet highly efficient miniaturized power supplies [2]. Given the drive for sustainable electronics, energy generation and delivery methods need to be integrated with the edge nodes in IoT networks. In addition, the high energy costs of fabricating batteries compared to their energy storage, [3], motivates solutions with a better end-to-end power generation, transfer and recovery efficiency.

Wireless Power Transmission (WPT) using rectifying antennas (rectennas), to either receive and convert dedicated power transmission or to recycle ambient radiation, is an attractive method of powering such IoT devices [1], [4]–[10]. Radio Frequency (RF) to DC rectifiers can be realized using μm-scale components based on a variety of semiconductors. However, antennas have a fundamental physical limitation on their size, where an antenna's physical aperture needs to be comparable to the wavelength to receive electromagnetic (EM) waves efficiently. At millimeter-Wave (mmWave) bands (30-300 GHz), high efficiency antennas can be realized at mm-scale, enabling efficient reception of EM waves by ultra-compact receivers for subsequent conversion to DC power [11]. mmWave WPT was initially proposed for the application of space power transmission [12], nevertheless, with the reducing power consumption of semiconductor devices, the battery-less pervasive IoT objective now drives recent developments in mmWave WPT.

A. REVIEW SCOPE AND STRUCTURE

mmWave power harvesting leverages the advances in mmWave antenna design and propagation measurements, rectifier design, modeling and matching techniques, in addition to high-frequency electronics packaging using both conventional and unconventional materials. This article presents a comprehensive review of recent advances in rectenna design for mmWave power harvesting. The

TABLE 1. Comparison of this review with recent review papers on wireless power harvesting.

Literature	Frequency bands	Focus areas
This review	mmWave (24-100 GHz)	• mmWave WPT fundamentals and the early beginning. • UHF and microwave vs. mmWave rectenna topologies. • Antenna design for mmWave WPT. • Rectifiers, discrete and integrated, for mmWave WPT. • Additive manufacturing and low-cost rectennas at mmWave. • Future mmWave EH research challenges.
Valenta *et al.*, 2014 [4]	UHF, Microwave and mmWave: (0.9-35 GHz)	• Rectifier modeling and characterization. • Rectenna impedance matching. • State of the art rectennas review.
Lu *et al.* 2015 [1]	UHF and Microwave	• Review of circuit design (Rectifier and power management). • Overview of single and multi-band antenna design. • SWIPT Protocols and techniques. • Communication Protocols in wireless-powered networks.
Soyata *et al.* 2016 [5]	UHF and Microwave	• Comparison of RFEH with other ambient EH methods. • RFID and Wake-up radios. • Rectifier impedance matching. • Power management design.
Guler *et al.* 2016 [6]	Sub-1 GHz UHF	• Rectifier performance metrics standardization. • Review of the rectifier topologies. • RFEH performance improvement through device-level and circuit-level design.
Shanawani *et al.* 2017 [7]	THz and sub-THz	• Photovoltaic PN junction cells vs. rectennas. • Rectification theory at THz. • Practical fabrication and manufacturing of THz rectifiers.
Divarkan *et al.* 2018 [8]	Microwave	• Overview of miniaturised antenna designs for RFEH. • Reconfigurable antennas, harmonic rejection and filtennas. • Rectifier topologies comparison.
Cansiz *et al.* 2019 [9]	Microwave	• RF Power sources. • Antenna arrays and flexible/wearable antennas. • Rectifier Impedance matching. • Rectifier topologies and power management comparison.
Wagih *et al.* 2020 [10]	Microwave	• Bandwidth and impedance matching • 50Ω RFEH antennas • Rectenna impedance matching • Radiation properties (gain and polarization) in RFEH

frequency spectrum covered in this work spans 24 to 100 GHz, the spectrum where emerging wireless networking applications have been proposed and are rapidly approaching commercial deployment. In this review, power "*harvesting*" is broadly defined as all efforts to recover DC power from an incident EM plane-wave at mmWave bands using a rectenna, regardless of the transmitter. "Recycling" of freely-available ambient power has been widely demonstrated at sub-6 GHz bands for GSM/LTE/Wi-Fi energy harvesting [13]–[15], along with spectral surveys of the power available for harvesting [13]. However, as mmWave cellular networks have not been widely deployed, rectennas have not been demonstrated harvesting cellular power at mmWave bands.

The review covers component-level and system-level aspects of mmWave WPT. First of all, the earliest implementations of mmWave WPT systems for space applications are reviewed, in Section II, and compared to modern mmWave power harvesting in the IoT context. We then review the motivation behind mmWave WPT from an end-to-end efficiency perspective, in Section III, analyzing the efficiency gains with directional systems. The review then discusses mmWave rectenna development and contrasts it to sub-6 GHz rectennas, outlining the typical architecture of rectennas and their building blocks in Section IV. Antenna design for rectennas is reviewed with an emphasis on size and gain trade-offs in Section V. Rectifiers are then analyzed theoretically and their design and matching techniques are reviewed in Section VI, comparing the advances and challenges in discrete Schottky-based and fully-integrated Complimentary Metal Oxide Semiconductor (CMOS) rectifiers. A holistic review of additively-manufactured and low-cost mmWave rectennas is presented in Section VII. Rectennas based on printable and flexible materials are reviewed comparatively and their application to mmWave-powered IoT is assessed. Finally, Section VIII discusses the

emerging research challenges related to antenna design for mmWave power harvesting as well as the unresolved issues hindering the wide-scale adoption of mmWave rectennas.

B. PREVIOUS WIRELESS POWER HARVESTING SURVEYS

Rectenna development builds upon a range of well-studied technologies. Several research communities have delivered significant advances which can be leveraged to enable a wireless-powered, and more specifically a mmWave-powered IoT. Therefore, it is essential to identify the existing surveys covering different aspects of wireless power harvesting systems. Table 1 summarizes the key focus points of recent reviews on wireless power harvesting, and compares them to this review. To begin with, antennas for RF power harvesting have been reviewed [1], [10]. It was shown that the bandwidth, gain and polarization of rectennas can vary depending on the application, whether it is ambient harvesting or directional WPT [10]. WPT systems with focus on rectifiers and their performance were extensively reviewed in [4], where it was shown that impedance matching, diode properties, and the frequency of operation limit the maximum achievable Power Conversion Efficiency (PCE). Power conversion and management circuits in RF power harvesting have also been reviewed [6], [16], exploring the impact of discrete and integrated rectifier topologies on the efficiency [6]. The advances in additive manufacturing for RF power harvesting and zero-power IoT were also reviewed, showing that RFID, back-scatter communications and passive UHF circuits are prime candidates for the battery-less IoT [17], [18].

None of the existing literature surveys have focused on mmWave WPT in the region between 24 and 100 GHz. THz-specific rectenna design methods and optical rectenna design were reviewed in [7], while touching upon Schottky-based rectennas in the lower mmWave bands.

II. SPACE POWER BEAMING: THE EARLY BEGINNINGS

W. C. Brown's earliest drone-powering rectennas operated at microwave bands below 10 GHz [19]. The additional atmospheric attenuation of mmWave signals due to air and water vapor was considered a major hindrance to mmWave WPT. Yoo and Chang were motivated by the miniaturization potential at mmWave to realize a rectenna operating at 35 GHz for space WPT applications [11], [20]. In space, mmWave signals will not be attenuated and hence high end-to-end efficiencies can be maintained with more compact transmitting arrays and rectennas. They developed a theoretical framework with numerical and experimental validation comparing the rectifier design process at 10 and 35 GHz [11]. Their theoretical analysis is used in Section VI-A to evaluate commercially-available diodes up to 100 GHz.

Although the 35 GHz rectenna in [11] achieved a 39% PCE, the maximum theoretical PCE of the rectenna is calculated to be 60%, if the antenna was matched to the rectifier's impedance to minimize the reflection. Therefore, it can be concluded that mmWave rectennas can be designed without an ideal impedance matching stage while still maintaining performance. The diode's cut-off frequency was calculated to be 155 GHz based on the parameters utilized in the simulation [11]. Therefore, harmonics propagation to the output could be ignored at 35 GHz. Hence the relatively-high 39% PCE can be achieved without stand-alone harmonic termination.

Rectenna development at mmWave bands by Koert and Cha was focused on presenting diodes of high breakdown voltage V_{Br}, to enable efficient reception of high power densities [12]. As with [11], Koert and Cha discussed the miniaturization potential of 35 and 94 GHz rectenna arrays for space applications, making higher gain antennas more realistic at mmWave compared to sub-6 GHz bands. They then developed rectennas in GaAs processes with fringed diodes with higher V_{Br}. Koert and Cha developed rectennas operating at 35 and 94 GHz [21]; 35 GHz is the frequency where the atmospheric attenuation reduces from the peak reached around 28 GHz, due to absorption by water-vapour. At 94 GHz, the rise in absorption at 60 GHz, due to oxygen, reduces to its lowest point above 50 GHz. The work by Koert and Cha was developed at an industrial lab (ARCO Power Technologies) which later became part of E-Systems and acquired by Raytheon Company, where the earliest WPT systems were developed [19]. Illustrations of power-beaming to earth are shown in [22], based on multiple issued patents by ARCO Power Technologies.

Following the feasibility studies showing the ability to realize rectennas beyond 30 GHz for mmWave WPT, the diode design was identified as a key challenge facing the development of mmWave rectennas [12]. The conclusion drawn about hybrid rectennas, i.e., a GaAs RFIC diode mounted on a printed circuit as opposed to a fully-integrated diode, is that hybrid rectennas are better suited for applications around 35 GHz. Beyond 94 GHz, a fully-integrated rectenna is essential. While the diode's junction would not be different in a fully-integrated rectenna, this shows that the critical bottle-neck to the rectenna is the parasitic capacitance introduced by the transition from a printed circuit to a GaAs die. The issue of estimating and factoring in the diode's packaging parasitics was revisited in more recent rectenna designs [23]–[25]. Parasitic capacitance of packaged devices is also more widely regarded as a challenge in mmWave components such as power amplifiers [26].

As interest in mmWave power harvesting has re-emerged for IoT applications [2], [27], it is essential to reflect upon the developments in high-power space WPT. The main difference between the work in [12], [20], [22], and practical commercial deployment of mmWave rectennas is the power densities. The high PCE, which approaches 90% in [11], requires a high mmWave power input, exceeding 10 mW/cm^2. While such an energy density is plausible in power beaming in space, it is highly impractical for WPT to IoT devices in a dense urban environment due to the limits on the Equivalent Isotropically Radiated Power (EIRP).

Thus, efficient rectification at mW and sub-mW power levels is essential to realize a mmWave-powered IoT.

III. MMWAVE POWER TRANSMISSION: THE END TO END EFFICIENCY

The channel efficiency is a function of the distance between the transmitter and the rectenna, the propagation medium, and the antennas' gain. The channel is often described as the bottle-neck of far-field WPT [28]. The end-to-end efficiency in WPT is given by

$$\eta = \underbrace{\frac{P_{RF}}{P_{DC}}}_{e_1} \times \underbrace{\frac{P_{RF-RX}}{P_{RF-TX}}}_{e_2} \times \underbrace{\frac{P_{DC}}{P_{RF}}}_{e_3} \times \underbrace{\frac{P_{DC-Load}}{P_{DC-RX}}}_{e_4}. \quad (1)$$

e_1 is the DC to RF efficiency at the transmitter and is a function of the oscillator and the power amplifier; amplifiers have been demonstrated with efficiencies around 50% (−3 dB) at mmWave bands [26]. e_2 is the channel efficiency and is a function of the transmitter and receiver gain, and the distance between them. Antenna gains can vary significantly but are typically between 0 and 30 dB. The path loss at mmWave bands exceeds 100 dB for 100 m separation, as low as 24 GHz. e_3 and e_4 vary significantly depending on the rectifier and power management circuit and can be over 50% [4], [6]. Therefore, it is clear that e_2 in (1) is the main challenge to be overcome in WPT.

As presented in [27] and [28], and widely advocated by W. C. Brown in his earlier wireless powering experiments [19], directional antenna arrays are essential to realize efficient power links in far-field WPT. In his review, W. C. Brown described the assumption that power density *always* decreased with the square of the distance as a "*widespread but incorrect assumption*" [19]. His conclusions were backed by the WPT efficiency e_2 approaching 100% using a beam guided using lenses and reflecting mirrors in 1961 [19]. While it is widely known that the path loss increases with the frequency-squared, we show that for a fixed transmitter and antenna physical size, the WPT efficiency e_2 increases with frequency.

In their theoretical analysis of mmWave energy harvesting in a cellular network context, Khan *et al.* concluded that WPT at 28 GHz can outperform that at 2.1 GHz [27]. Their conclusion builds on the assumption that large directional antenna arrays can be used at the base-station, at 28 GHz, which increases the power received by an energy harvester. Furthermore, when considering empirical channel models, it was found that for an average distance of 113 m between the base-station and the nodes, the received power could be increase by 2× over 2.1 GHz using a 16 antenna base-station at 28 GHz, for the same transmitted power level.

For a fixed transmitter antenna size, an increase in frequency results in a narrower beamwidth and subsequently higher gain. When the transmitter is aligned with the receiver, this results in increasing WPT efficiency with frequency [29]. To illustrate the gain G improvements, and subsequently the received power, at mmWave bands, we consider a transmitter and a receiver of a fixed physical area A of 100 cm^2, at 100 m separation d. An ideal aperture efficiency $\eta = 1$ is assumed. Using the antenna's aperture efficiency η, the maximum achievable gain can be calculated based on the effective area. The maximum achievable gain is given by

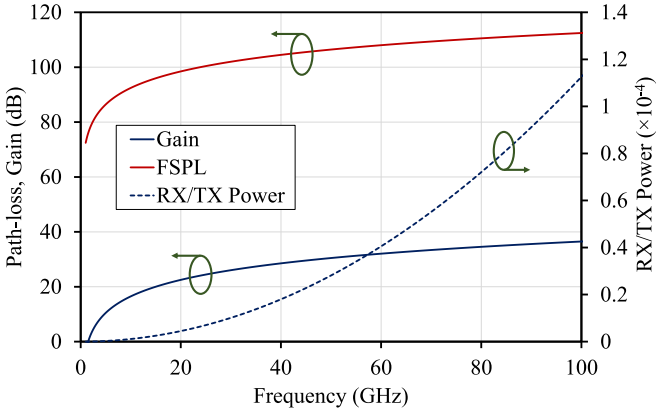

FIGURE 1. Calculated propagation losses and gain from 1 to 100 GHz and the received power ratio for directional transmitter and rectenna.

$$G = \frac{4\pi\eta f^2}{c^2} A, \quad (2)$$

where f is the frequency and c is the speed of light [30]. The received to transmitted power ratio can then be calculated based on the free space propagation loss (FSPL) formula,

$$\frac{P_{RX}}{P_{TX}} = G_{TX} G_{RX} \left(\frac{c}{4\pi df}\right)^2 \quad (3)$$

The FSPL formula can be rewritten after substituting the antennas' gain calculated using (2) giving

$$\frac{P_{RX}}{P_{TX}} = \frac{1}{c^2 d^2} A_{TX} A_{RX} \eta_{TX} \eta_{RX} f^2. \quad (4)$$

Hence, it can be seen from (4) that assuming a fixed transmitter and receiver size, the WPT efficiency increases with frequency. Eq. (4) gives a physical explanation to the higher power received by a "large" mmWave WPT system in [2], [29], [31] compared to UHF bands. Fig. 1 shows the calculated P_{RX}/P_{TX} for the 10×10 cm^2 transmitter and receiver at $d = 100$ m. This calculation does not account for additional atmospheric attenuation at mmWave bands, which results in reduced penetration capabilities [32]. However, the attenuation is less than 1 dB/km below 50 GHz and above 60 GHz [31].

The exponentially-increasing WPT efficiency with frequency is however hindered by many other practical challenges. For example, rectifiers suffer from multiple physical limits which constrain their high-frequency PCE [4], [11]. In addition, antennas' conductive and dielectric losses increase with frequency and can limit mmWave antennas to very low-loss substrates and conductors. These challenges are reviewed in the next sections.

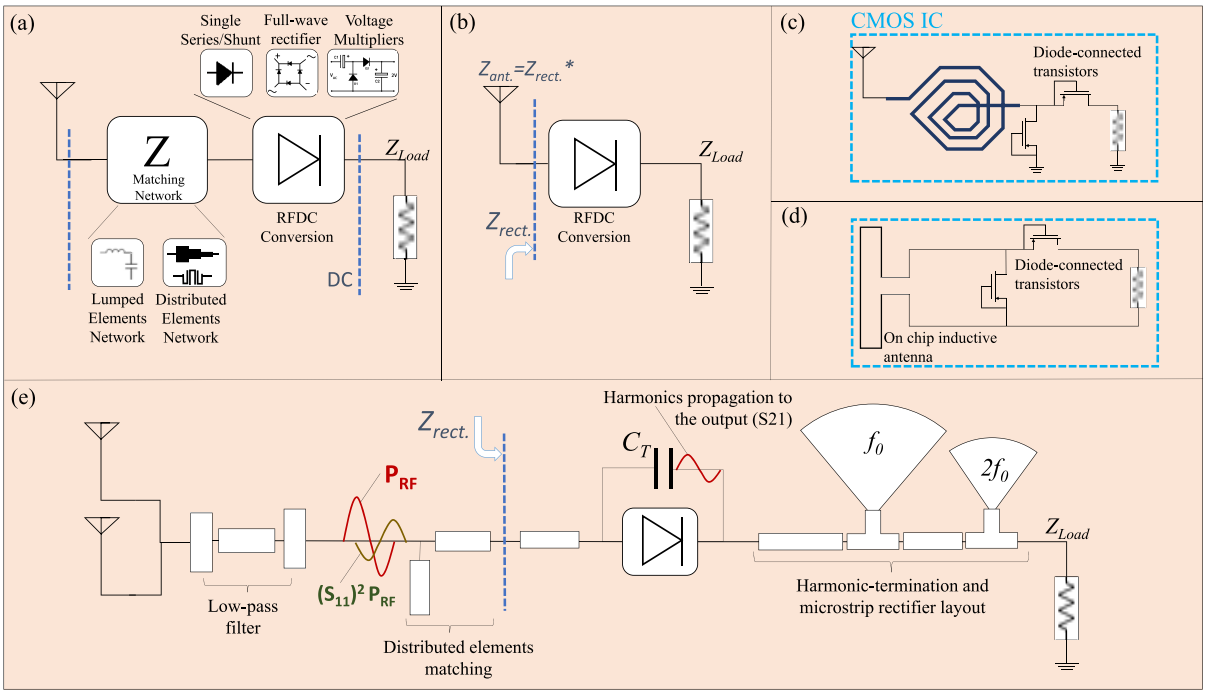

FIGURE 2. The typical rectennas topologies: (a) sub-6 GHz rectenna with a 50Ω antenna and a matching network, (b) sub-6 GHz rectenna with antenna-rectifier co-design, (c) mmWave fully-integrated rectenna with on-chip matching, (d) fully-integrated mmWave rectenna with no standalone matching stage (e) Schottky-based mmWave rectenna, showing the rectifier's parasitic capacitance and the harmonic-termination microstrip stubs at the output.

IV. THE RECTENNA AT MMWAVE BANDS

The typical rectenna is formed of an antenna, a rectifier and a matching network. Alternatively, a high-impedance antenna can be designed to directly match the rectifier [10]. In sub-6 GHz networks, the matching topology and source-load impedances determine the rectenna's PCE [33]–[35]. However, at mmWave bands, where diodes approach their cut-off frequencies and packaging and layout parasitics cannot be ignored, harmonic termination and low-pass filtering play a dominant role in determining the rectenna's performance. Fig. 2 shows the structure of a typical Ultra-high Frequency (UHF) or Microwave rectenna and a mmWave rectenna.

Microwave rectenna impedance matching is achieved using lumped or distributed matching networks [15], [33], [36], and antenna rectifier co-design [35], [37]–[39], shown in Fig. 2-a and b respectively. The main focus is on maximizing the PCE through minimizing the S_{11} at the antenna's interface, as well as improving the voltage level at the input which reduces the rectification losses. The mmWave rectenna, in Fig. 2-e, requires additional components to prevent the high frequency harmonics from propagating to the output. The diodes' non-linearities are more evident and can result in significant power being generated at higher harmonics, which, if not terminated properly, can adversely lower the DC output [40]. In addition, the rectifier design, simulation and matching stages are more uncertain and discrepancies between the datasheet and real-world performance need to be tackled. Fig. 2-e shows the additional components of a mmWave rectenna such as filters and harmonic termination, often not seen in sub-6 GHz rectennas, as well as the main challenge, the integration of the antenna and the rectifier at the $Z_{Rect.}$ plane.

The rectifier/antenna interface ($Z_{Rect.}$ plane in Fig. 2-e) is the main source of uncertainty. mmWave rectenna design can involve multiple design iterations to experimentally characterize the rectifier's impedance and diode parameters [23]. It is also not uncommon to see additional prolonged antenna or rectifier feed-lines [41], [42], modified designs post-fabrication [43], as well as a generally higher discrepancy margin between simulation and measurements [25], [44]. The antenna and rectifier design are commonly treated as separate matters and are reviewed separately in Sections V and VI.

Fully-integrated rectennas at mmWave bands, motivated by the miniaturization of the antenna, follow a different architecture. Given the sub-mm scale of CMOS ICs, the parasitics of the entire system are significantly lower and hence harmonic termination and layout consideration are not of great significance as in discretes. On-chip antennas are also different in their design requirements where balanced antennas are more common than in discrete rectennas. Furthermore, more attention is given to circuit-level simulation to extract the rectifier's input impedance compared to discrete rectennas, where it is not possible to prototype and measure the rectifier separately. Integrated antenna design for mmWave rectennas is reviewed in Section VI-B.

TABLE 2. Comparison of antenna designs proposed for rectennas beyond 20 GHz.

Rectenna	Frequency	Antenna Design	Peak Gain (dB)	−3 dB beamwidth (°)	Polarization	Dimensions (mm)	Substrate/ Technology
2014 [45]	21 GHz†	Co-planar strip dipole	>4	>50	Linear	10×13	RO6002
2014 [46]	24 GHz*	4×4 SIW array	15	≈15	Linear	75×35	Duroid 5880
2014 [23]	24 GHz*	2×2 cavity-backed array	12.6	≈20	Circular	30×30	Duroid 5880
2015 [47]	24 GHz*	Folded dipole	−1	>60	Linear	3.7×1.2×0.12	65nm CMOS
2017 [48]	24 and 40 GHz*	DRA on slot antenna	−1 at 24 GHz, 0 at 40 GHz	65 at 24 GHz, 360 at 40 GHz	Linear	32×32×4.64	DRA on CMOS
2017 [24]	24 GHz*	2×2 microstrip patch array	5	≈30	Linear	12×12	LCP
2019 [49]	22-28 GHz*	2×1 microstrip patch array	NR (<5)	>50	Linear	NR: ≈10×10	Printed FLGR02 (tanδ=0.03)
2019 [50]	28 GHz*	8×5 Rotman lens array	≈18	80	Linear	55×87	LCP
2020 [51]	24 GHz*	4×4 microstrip patch array	13.8	<20	Linear	60×30*∗	RO3003
2020 [44]	24 to 40 GHz*	Single antipodal Vivaldi	>8 up to 30 GHz	50	Linear	16.5×9.5	Textile (tanδ=0.026)
1992 [11]	35 GHz*	Stripline dipole	NR	NR	Linear	NR: ≈5×3	Duroid
2014 [52]	35 GHz*	4×4 patch	19‡	18	Linear	21.7×22.6	Duroid 5880
2016 [43]	35 GHz*	Fabry-Perot resonator	17	NR	Circular	32×32×4.64	Waveguide (air-filled)
2020 [53]	35 GHz*	Waveguide Fabry-Perot antenna	15.1	≈15	Linear	17.7 × 17.7 × 2.2	Waveguide (air-filled)
2016 [54]	60 GHz*	2×2 Grid array on package	8.9	≈15	Linear	10×10×0.5	CCL-HL832MG package (tanδ=0.012)
2018 [55]	60 GHz*	8×1 microstrip array	13.3‡	≈20	Linear	18×7.8×0.2	Thin film ceramic
2013 [56]	71 GHz*	λ/4 monopole	NR	NR	Linear	0.94×0.75	65 nm CMOS
2015 [25]	94 GHz*	Coplanar Bow-tie	3.9‡	≈20	Linear	2×2×0.1	Thin film alumina
2018 [57]	94 GHz*	8×8 Microstrip	9	≈25	Linear	7×15	NPC F220A
2014 [58]	75-110 GHz *‡	Meander dipole	2.28‡	>180	Linear	0.53×0.91	65 nm CMOS

*50Ω antenna bandwidth; †complex impedance antenna; ‡simulated only; NR: not reported.

V. ANTENNA DESIGN FOR MMWAVE RECTENNAS

To counter the high propagation losses and the additional atmospheric attenuation, mmWave rectennas rely on high gain antennas to maximize the harvested power. A variety of antenna design and fabrication methods have been reported in literature, from wave-guide, to Printed Circuit Board (PCB), and fully-integrated antennas in CMOS processes. In this section, recent trends and advances in antenna design for mmWave rectennas are reviewed. Section VII is dedicated to additively-manufactured antennas and rectennas on low-cost substrates, where they are reviewed from a holistic rectenna perspective rather than being purely focused on the antenna design.

Table 2 compares the antenna designs integrated in rectennas operating above 20 GHz. The antennas in the table can mostly be classified into passive antennas and arrays, as well as passive rectenna arrays with beamforming networks. These implementations are then reviewed in detail in the next subsection. Fully-integrated on-chip antennas, implemented in CMOS processes, as part of rectennas or complete mmWave-powered systems are also included in the table. In the substrate column, the dissipation factor (tanδ) of lossy and unusual materials, such as textiles and printable dielectrics, are included. Where the dielectric properties are not quoted, tanδ is <0.001 and the material's properties are available from the manufacturer's datasheet.

While sub-6 GHz rectennas have been demonstrated based on both 50Ω antennas and co-designed high-impedance antennas [10], the majority of mmWave antennas have been matched to $Z_0 = 50\Omega$. Hence, the bandwidth is typically quoted as the antenna's 50Ω $S_{11}<-10$ dB bandwidth. The only implementation of a high-impedance antenna directly matching the rectifier, beyond 20 GHz, was presented in [45].

A. ANTENNAS AND ARRAYS IN MMWAVE RECTENNAS

High and medium gain antennas have historically been developed using waveguide components and horn antennas, due to their high power handling capabilities and low losses [59]. mmWave rectennas have been developed based on waveguide antennas [43] or with a waveguide-to-microstrip interface for integration with waveguide components [53]. Such rectennas will have the highest gain which

exceeds 15 dB, as in Table 2, and can be demonstrated with linear, [53], or circular polarization [43]. Circular polarization may be preferred in WPT applications to overcome the angular misalignment between the transmitter and the rectenna [10], [23], [53], [60]. However, it is critical that the propagation path does not include reflections or the circular polarization will not be received.

On the other hand, waveguide components are 3-dimensional and more expensive compared to planar antennas. Arrays are the most common method to improve the directivity of microstrip antennas [61]. The majority of PCB antennas in Table 2 are based on arrays with at least two elements [49], and as many as 4×4 elements [46], [52]. However, a single element reflector-backed antipodal antenna [44], on a textile substrate, demonstrated higher gain than other microstrip patch arrays [24] while occupying a smaller area. While patch antennas have the advantage of not requiring vias, a via may still be required at the rectifier stage. Although microstrip patch antennas can achieve high gain and radiation efficiency on low-loss substrates, they are inherently narrow-band, especially when implemented on thinner substrates [23]. Another advantage of planar microstrip antennas is that they can be realized on a variety of unconventional substrates using printing and photolithography [17]. Antennas implemented on lossy substrates and using additive manufacturing are reviewed in detail in Section VII.

The development of Substrate-Integrated Waveguide (SIW) transmission lines has significantly advanced the development of planar antennas at mmWave bands. SIW antennas benefit from suppressed surface waves which improves the antenna elements' isolation, and subsequently the radiation properties [23], [62]. A 4×4 rectenna array was proposed in [46] based on the SIW slot array detailed in [63]. To interface the SIW with the microstrip rectifier in [23], a SIW-microstrip transition was developed. The length of the tapered transition microstrip line is 16.7 mm (1.33λ) highlighting that a standard SIW transition can significantly increase the area of a mmWave rectenna. To reduce the size of SIW rectennas, a 24 GHz rectenna was realized in a 15×22.9 mm^2 area based on a rectifier integrated inside the SIW cavity [64]. A vertically-stacked double-element rectenna based on two 10 dBi 35 GHz SIW Vivaldi antennas with microstrip rectifiers was proposed in [65].

While SIW rectennas have only been implemented on low-loss high-frequency substrates [23], [46], [64], [65], SIWs have previously been demonstrated on unusual substrates. For wearables, SIWs based on conductive threads were used to realize low-loss high-isolation SIW antennas and transmission lines for wearable applications [66]. Rigid threads woven into fabrics have been used to demonstrate transmission lines up to 37 GHz [67], the proposed textile waveguide to standard waveguide transition allows the development of mmWave rectennas based on SIW textile antennas integrated with microstrip components such as rectifiers [44].

B. FULLY-INTEGRATED ANTENNAS

At mmWave bands, the miniaturization of antennas enables their integration in standard CMOS processes or semiconductor packages with the associated communication [68], or in this case energy harvesting, circuitry. Multiple on-chip antennas have been proposed for mmWave rectennas and mmWave-ID [47], [48], [54], [56], [69]. Fig. 9 shows the micrographs of reported on-chip antennas for power harvesting in the 24 to 94 GHz spectrum.

Folded dipole antennas were used for 24 GHz fully-integrated rectennas for RFID applications [47], [69]. With a length of 1.6 and 3.7 mm for [69] and [47], the dipoles achieve a gain of -8.7 and -1 dB, respectively. As [47] uses the 60 GHz band for up-link, a $\lambda/2$ dipole was integrated on the same chip for communications at 60 GHz. In CMOS, differential balanced antennas such as dipoles are generally preferred to single-ended ones, dipoles can connect to differential circuits eliminating baluns [68]. Such implementations enable fully-integrated pad-less radio transceivers, which do not require any external components to function. To account for the multi-antenna integration in [47], the positioning of the 60 GHz antenna and the energy storage capacitors (shown in Fig. 3-a) was optimized to prevent mutual coupling with the 24 GHz dipole. The 24 GHz dipole had a simulated impedance of 60Ω and a radiation efficiency approaching 30% [47].

A similar design was presented in [56] with an on-chip 71 GHz $\lambda/4$ monopole. The antenna was directly connected to a single-ended inductive-matched rectifier, as shown in Fig. 3-c. Although the gain was not reported, it is expected that the antenna's gain approaches 0 dB as with [47], as the monopole is $\lambda/4$ in length. A comparison of CMOS mmWave power harvesting antennas [47], [56], [69] was presented in [2] concluding that the Q-factor of the matching component is equally significant to the antenna's dimensions when evaluating the performance, in terms of received DC power, of mm-sized far-field power receivers.

C. BEAMFORMING AND PHASED ARRAYS

In 5G and mmWave communications, phased array controllers are employed to steer the main beam of the receiving antenna. Phased array transceivers have been proposed with low power consumption down to 10s of mW for active reception [71]. Such power overhead is mainly due to the amplifiers in the system but also due to the tunable phase-shifters. In a mmWave rectenna aimed at high-power applications, such overhead for phased-array tuning could be accommodated without significantly reducing the net DC output. However, for low-power harvesting systems, complex active array tuning circuits are not feasible and hence mmWave rectennas (Table 2) did not employ phased arrays.

In [72], a method of employing a rectenna to tune a phased antenna array was proposed at 60 GHz. Although the rectifier's performance is not discussed in details, the radiation patterns of the retro-directive array can be reconfigured successfully from a mmWave incident power density of

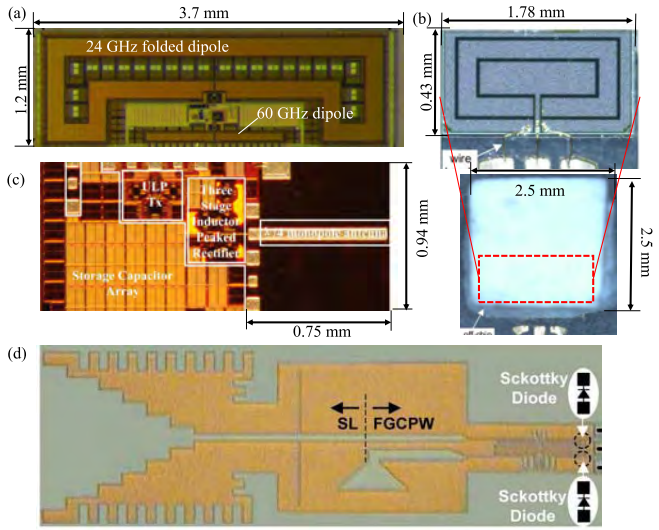

FIGURE 3. Micrographs of the on-chip energy harvesting and mm-ID antennas: (a) 24 GHz folded dipole rectenna and 60 GHz λ/2 communications dipole, reproduced from [47], (b) 71 GHz λ/4 monopole rectenna with inductor matching, reproduced from [56], (c) 24/40 GHz slot with off-chip dielectric resonator, reproduced from [48], (d) 35/94 GHz (2.9 mm^2) rectenna, reproduced from [70].

0.013 mW/cm^2, providing a bias voltage of 5 V and allowing the local oscillator to produce 5 dBm of power. Such efforts could be combined with more recent low-power phased-array controllers to realize a steerable phased array rectenna for long-range high-power mmWave WPT.

Beamforming on the other hand allows quasi-omnidirectional energy harvesting using high gain antenna arrays and a Multi-In Multi-Out (MIMO) beamforming network [50]. Beamforming techniques were used for sub-6 GHz energy harvesting based on full RF combining with a butler matrix and 1×4 patch antenna arrays at 2.4 GHz [73]. Low-loss coaxial cables are used to connect the 3D cylindrical patch array to the butler matrix which connects directly to the rectifiers [73]. The system in [73] achieves wide angular coverage with four main beams each having over 6 dB higher gain compared to dipoles. Nevertheless, the structure is very complex and requires low-loss interconnects as well as occupying a large volume ($290 \times 130^2\pi$ mm^3). At mmWave bands, implementing such large area arrays is straightforward on planar flexible substrates [50], [74]. Therefore, beamforming networks can enable long-range wide-beamwidth energy harvesters beyond 24 GHz.

VI. DIODES AND RECTIFICATION

A. SCHOTTKY DIODES AT MMWAVE BANDS

A rectifier's PCE is limited by the forward bias threshold voltage V_F at lower power levels, and by the breakdown voltage V_{Br} at higher power levels. An additional loss is incurred due to the harmonics generated due to the non-linearity of the diode [11]. At mmWave frequencies, the fundamental-tone and harmonics propagation to the output becomes the major limiting factor to the PCE, due to approaching the cut-off

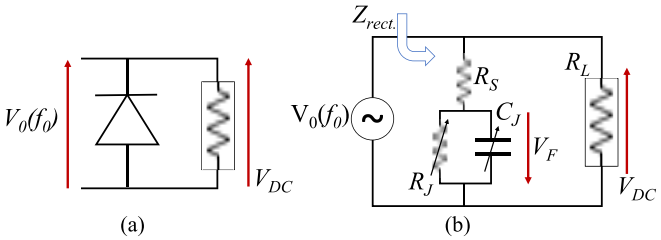

FIGURE 4. The shunt diode model used in the theoretical analysis proposed in [11]: (a) shunt diode and load configuration, (b) diode equivalent circuit model.

frequency of the diode. It was found that a significant proportion of the input power (66%) can exist at the first and second harmonics at the output of the rectifier, with only 32% of the output power being DC [40]. Most commercially-available silicon (Si) Schottky diodes have a junction cut-off frequency around 20 GHz, which can be adversely reduced by the packaging and mounting parasitics. Therefore, Gallium Arsenide (GaAs) diodes, capable of switching beyond 100 GHz, are typically chosen for rectennas beyond 20 GHz.

We use the proposed technique by Yoo and Chang in [11] to evaluate the theoretical PCE of rectifiers based on commercial diodes. The solution to the equations in [11] was obtained using MATLAB adapted from the methods used by Valenta and Durgin in their review [75], and described in [76], [77]. In this analysis, the RF input is modeled as a voltage source of magnitude V_0. The calculated PCEs are theoretical maximums and exclude any impact of the antenna's impedance and assume no impedance mismatch at the rectifier's input; a discussion of the accuracy of this method is presented in [77]. To first discuss the antenna's power output as a voltage source, for a conjugate-matched small and simple antenna, the voltage V_0 corresponding to the collected power, P_{RX} is given by

$$V_0 = \sqrt{4(\Re\{Z_{Ant.}\})P_{RX}}, \tag{5}$$

where the real component of the antenna's impedance $Z_{Ant.}$ is the summation of the radiation and loss resistances, respectively [78].

The diodes are evaluated in shunt configuration, as in Fig. 4-a, with a resistive load. When the diode is on, the voltage drop across the diode is equal to the forward junction threshold voltage of the diode V_F as in Fig. 4-b. For $V_1 < V_{BR}$ (the diode's breakdown voltage), the diode's PCE is defined in [11] as

$$PCE_{\text{Diodes}} = \frac{P_{\text{DC}}}{P_{\text{Loss}} + P_{\text{DC}}}, \tag{6}$$

where P_{DC} is the power across R_L and P_{Loss} is the power dissipating through the diode.

The diodes are modeled based on the junction parameters only excluding packaging parasitics. This however, assumes accurate characterizations from the manufacturer and an assembly process of the rectifier that matches the measurement setup by the diode maker. The junction parameters define the maximum usable frequency of the diode, i.e.,

TABLE 3. Properties of the Schottky diodes evaluated analytically.

Diode	SC	C_J (pF)	R_S (Ω)	V_F (V)	V_{Br} (V)
SMS7630 [33]	Si	0.2	20	0.14	2
MA4E [24]	GaAs	0.045	5.1	0.	9
W-ZBD [25]	GaAs	0.019	13	0.075	6
MS8150-P2613 [81]	GaAs	0.065	4	0.7	4.0

the cut-off frequency $f_{\text{cut-off}}$. In Schottky diodes, $f_{\text{cut-off}}$ is defined as the frequency at which the resistive and reactive components of Z_{Rect} are equal, and hence the output is halved (−3 dB loss) [79], [80]. $f_{\text{cut-off}}$ is given by

$$f_{\text{cut-off}} = \frac{1}{2\pi R_S C_T}. \tag{7}$$

The simple closed-form equation (7) can be used to quickly evaluate the suitability of commercial diodes for mmWave rectification based on their total capacitance $C_T = C_J + C_{\text{Package}}$. Packaging parasitics were found to reduce the maximum usable frequency of diodes by up to 50% [44].

Four commercial diodes are considered based on the theory in [11] to evaluate their PCE_{Diode}. The diode models and parameters are given in Table 3, along with references to studies discussing the extraction of the diodes' properties, and the use of the extracted parameters in the rectenna design and simulations. Diode and rectifier characterization are discussed in more detail in Section VI-C.

Fig. 5 shows the maximum achievable PCE_{Diode} of the four diodes for varying frequencies. Such frequency sweep was previously presented in [11] and [4] but using a single independent variable $\omega R_S C_J$, which combines the frequency $\omega = 2\pi f$, and the diode's parameters R_S and C_J, all of which contribute to the phase delay [11]. In addition, both [11] and [4] considered an ideal diode with $V_F = 0$ and $V_{Br} = \infty$. Considering real diodes, as in Fig. 5, enables clear visualization of the impact of frequency on PCE_{Diodes}, and the significance of parameters such as V_F at frequencies approaching $f_{\text{cut-off}}$.

While it can be seen that a diode with very low parasitics and V_F such as the Virginia Diodes W-band ZBD (Zero-Bias Detector) Schottky diode will always achieve the best PCE at low input voltages and very high frequencies, such devices may be impractical in commercial IoT due to the diode's cost of up to \$100, 15× higher cost than other GaAs diodes such as the MA4E. An interesting case in Fig. 5 is that where $V_0 = 0.1$ V and $R_L = 100\Omega$, it can be seen that the SMS7630, despite having $f_{\text{cut-off}}$ around 24 GHz, achieves higher PCE_{Diode} up to 25 GHz compared to the MS8150 whose $f_{\text{cut-off}}$ exceeds 60 GHz. This highlights that although a trade-off exists between having a low R_S and a low V_F, a diode whose V_F is high cannot be used to harvest low power efficiently. In [44], the SMS7630 was simulated using Harmonic Balance (HB) with and without the packaging parasitics where it was found that based on the maximum parasitics, the diode cannot be used for rectification at 24 GHz. Characterizing Schottky diodes at mmWave bands is challenging and can require a combination of DC and mmWave measurements to accurately capture the large-signal response [24], [25], [82].

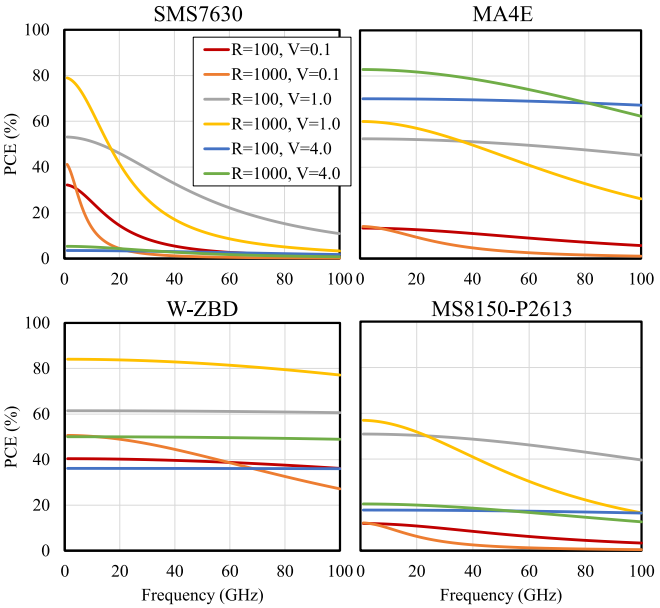

FIGURE 5. Calculated maximum achievable PCE for varying incident frequency, of voltage magnitude V and load *R*, for commercial Schottky diodes.

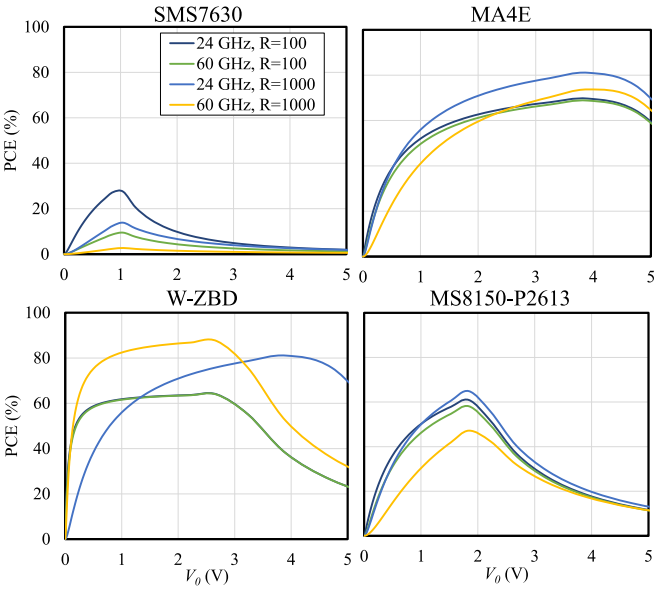

FIGURE 6. Calculated maximum achievable PCE for varying V_0 at 24 and 60 GHz with a load *R* for commercial Schottky diodes.

The theoretical analysis was used to analyze the impact of varying input voltage (i.e., mmWave power) on the PCE, at 24 and 60 GHz, and for 100Ω and 1000Ω loads. Across all diodes and loads, the low-power (V_0<1 V) PCE decreases with increasing frequency. While a higher R_L to R_S ratio improves the PCE when $V_0 < V_F$, it limits the high frequency performance [11]. This is particularly noticeable below 24 GHz, in Fig. 5 and 6, where a 1000Ω load improves the PCE.

Other than commercially-available Schottky diodes, multiple diodes have been proposed in literature showing potential for efficient rectification at mmWave bands. In [83], although the low-barrier tunnel diode was demonstrated at 2.4 GHz with the highest low-power (sub −30 dBm) PCE surpassing commercially-available diodes, measurements show that the diode can be used for efficient rectification beyond 40 GHz. From the Vector Network Analyser (VNA) impedance measurements at −30 dBm, the diode maintains a predominantly reactive impedance showing the potential for mmWave rectification. In [84], a self-switching graphene diode was proposed and integrated with a 2×2 patch antenna array on a silicon/silicon-dioxide substrate. For a 50Ω probe-feed, the diode has a voltage sensitivity (responsivity) of 7.04 V/W at 28 GHz from a 1.22 mW input [84]. In [81], a Mott diode was used in a 93 GHz rectenna, showing over 5× PCE improvement over the Microsemi MS8151. However, as compared in Fig. 5, the MS8151 does have a very high V_F which exceeds that of the MS8150 compared in Fig. 5, and shown to have the lowest PCE compared to other GaAs diodes such as the MA4E and the ZBD.

B. FULLY-INTEGRATED RECTIFIERS

CMOS rectifiers have been widely used for fully-integrated on-chip RF-DC conversion at sub-6 GHz and mmWave bands. The high $f_{\text{cut}-\text{off}}$ of CMOS diode-connected transistors enables efficient rectification at mmWave bands. Furthermore, the fully-integrated nature of the devices implies no influence from the packaging parasitics, which were previously shown to significantly reduce $f_{\text{cut}-\text{off}}$ of Schottky diodes [24]. However, such parasitics will still exist once a CMOS rectifier is integrated with a PCB antenna. On the other hand, multiple CMOS mmWave rectifiers were reported with power-sensitivity (on-wafer) below 0 dBm [47], [54], which is not typically achieved by discrete Schottky-based rectifiers.

As shown in Table 2, multiple antennas have been proposed in CMOS processes to enable improved integration of mmWave rectifiers. For example, at 24 GHz a folded dipole antenna was directly connected to the CMOS rectifier in [47] without separate impedance matching. At 62 GHz [85], and 71 GHz [56], Gao *et al.* proposed an inductor-peaked rectifier for threshold voltage cancellation. The series inductor connecting the gate of the diode-connected transistor was used to resonate with the transistor's capacitance. A series inductor was also used to match the rectifier showing a $S_{11}<-20$ dB bandwidth from 54 GHz to over 64 GHz. The design of fully-integrated CMOS mmWave-powered systems is described in detail in [86]. Another topology used for rectification at 60 GHz is a cross-coupled rectifier [54]. The flip-chip CMOS rectifier was connected to a grid array antenna-on-package with a transformer balun resulting in a predominately real rectifier impedance, which results in resonance at the operation frequency.

TABLE 4. Comparison of rectifiers and matching networks in CMOS.

Lit.	Freq. (GHz)	Z-match	Process	1 V Sensitivity	Max PCE
[69]'14	24	Parallel inductor	180nm	−2	1%*
[47]'15	24	Folded dipole	65nm	−10	NR
[54]'16	60	Transformer balun	40nm	6	28%
[85]'13	62	Series inductor	65nm	−4†	7%
[56]'13	71	Series inductor	65nm	5.2	8%

*Calculated from DC voltage across 1 MΩ load; †estimated.

Table 4 compares the recent mmWave CMOS rectifiers. All the rectifiers were realized in standard digital CMOS processes. This allows for large-scale low-cost production of high-efficiency rectifiers operating above 60 GHz. In addition, the 60 GHz power amplifier, with 24.6 dBm output, demonstrated by [54] as part of a complete WPT system shows that complete mmWave WPT can be realized in standard digital CMOS as well as integrated with off-chip compact antennas. As opposed to Schottky-based rectennas (Fig. 2), discussed in the next section, a harmonic termination or low pass filtering stage was not required to realize high-efficiency rectifiers, due to the high level of integration, high $f_{\text{cut}-\text{off}}$ and overall compactness.

C. DESIGN AND MATCHING OF MMWAVE RECTIFIERS

To achieve high PCE, it is essential to match the impedance of the generator (i.e., the antenna) to the rectifier's input impedance at the frequency, load current, and power level of interest. At UHF and microwave, this could be achieved using antenna rectifier co-design or impedance transformers [10]. As shown in Fig. 2, Schottky-based mmWave rectennas often have a standalone impedance matching stage, and the antenna or array are matched to 50Ω characteristic impedance. The key challenge in matching rectennas at mmWave bands is obtaining an accurate estimate of the diode's parameters, especially the packaging parasitics. Such knowledge will enable the use of commercial simulation software and non-linear circuit analysis methods such as HB to evaluate the optimum $Z_{rect.}$ at the rectifier's transition plane. The transition plane, shown in Fig. 2, marks the transformation of the 50Ω antenna impedance to the rectifier's. Furthermore, the rectifier design will include additional stages when designing the "DC" side of the circuit to properly terminate the harmonics and prevent PCE degradation. The layout of the circuit beyond the diode will still significantly impact the input impedance and the propagation of harmonics to the output.

Several methods have been proposed in literature to realize the components shown in Fig. 2-e, the layout of selected rectifier implementations in literature is reproduced in Fig. 7. The key difference between the implementations is how the

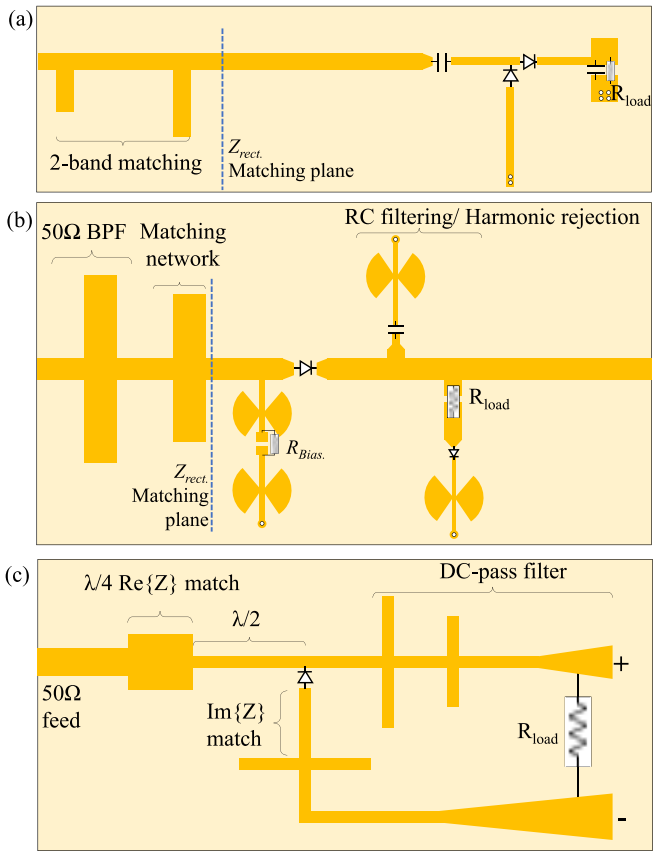

FIGURE 7. Layout (not to scale) of Schottky-based rectifiers reported in literature showing the main components: (a) Dual-band 28 and 38 GHz voltage doubler [42], (b) self-biased 24 GHz rectifier [23], (c) 35 GHz shunt rectifier [43].

matching network is realized, and how the DC output is filtered.

The theoretical analysis provided by Yoo and Chang's mmWave rectenna can be used to evaluate the input impedance of shunt diodes using closed form equations [11]. At 10 GHz, the theoretical calculations have shown a good agreement (<10% discrepancy) between the calculations and Method of Moments (MoM) simulations. However, at 35 GHz the discrepancies increase to approximately 50%. The MoM simulations showed a close agreement with the measurements for a 400Ω load but not for a 100Ω load. This demonstrates that the higher-current diode parameters were not characterized as accurately as the low-current ones. Yoo and Chang attributed the discrepancies and the lower efficiency at 35 GHz to impedance mismatch. As the S_{11} of the rectifier was not measured due to the coplanar structure which is hard to interface with a single-ended VNA, it is hard to evaluate the impedance matching of the 35 GHz rectifier. On the other hand, using a tunable open stub tuner at 10 GHz has improved the 10 GHz rectenna's PCE from 45% to over 60% to approach the theoretical maximum. This supports the assumptions that the 35 GHz rectenna was limited by an impedance mismatch at the diode interface. Finally, it is key to note that the rectifier had a fairly simple layout with no open stubs terminations and only used a DC-pass filter to prevent high frequency components from propagating to the output.

In more recent rectenna implementations by Ladan *et al.* [23], [40], [82], a more empirical approach was adopted to design and match the rectifier. The rectifier was first designed including harmonic termination at the fundamental tone f_0 and the second harmonic $2 \times f_0$. To account for the high Electrostatic Discharge (ESD) susceptibility of GaAs diodes, ESD protection was included using a shunt 200 kΩ resistor at the diode's input. To minimize the influence of the ESD protection on the mmWave signal path, λ/4 at f_0 butterfly radial stubs were added to the ESD protection branch. Including ESD protection is essential especially for the GaAs diodes which are the most costly component in the system and are difficult to replace. Yet, apart from [40], ESD protection remains uncommon in mmWave rectennas which use highly ESD-sensitive devices. At 94 GHz, Hemour *et al.* used both on-wafer measurements, with a TRL calibration, and DC IV-curve measurements to measure the VDI W-ZBD characteristics [25]. Nevertheless, the performance of the rectenna was underestimated in simulation due to over-estimating the diode's parasitics based on the empirical characterization [25]. At 24 GHz, Bito *et al.* used DC IV curve measurements to optimize the models of the MA4E1317 [24]. As with [25], the rectifier's measured output surpassed that of the HB simulation model due to over-estimation of the diode's losses [24].

When considering the distributed microstrip layout of the rectifier in [40] after adding the harmonic termination, ESD protection, and in [40]: the extra stage for harmonics recycling, the rectifier's impedance can no longer be analyzed using simple analytical formulas as in [11]. To explain, the size of the rectifier and the additional component will result in multiple Smith chart rotations significantly varying the diode's impedance at individual tones. As a result, Ladan *et al.* resorted to fabricating Through-Reflect-Line (TRL) calibration standards on the same PCB. The bespoke calibration "kit" is then used to transfer the VNA calibration plane to the rectifier's input (the $Z_{rect.}$ plane in Fig. 7-b) allowing the coax-microstrip transitions to be calibrated out. The VNA is then used to directly measure Z_{rect} for which a microstrip matching network is then designed and implemented on a second PCB. As the rectifier is matched to 50Ω, a standard band-pass filter (BPF) was added between the patch array and the matching network. The measured S_{11} of the rectifier shows a good impedance match at both the design frequencies of 24 and 35 GHz in [23] and [40], respectively.

In a more recent rectifier design at 35 GHz, Bozzi *et al.* proposed a shunt-diode rectifier based on microstrip series matching [43]. The microstrip feedline connecting the shunt diode to the negative DC terminal of the rectifier was responsible for canceling the rectifier's capacitance at 35 GHz, as measured using a VNA. A λ/4 impedance transformer is then used to transform the real impedance of the diode.

TABLE 5. Comparison of reported Schottky rectifiers and matching networks.

Lit.	Freq. (GHz)	Z-match	Harmonics Termination	1 V Sensitivity	Max PCE
[23]'14	24	L-microstrip	radial stubs at f_0, f_1	9 dBm	37%
[51]'20	24	L-microstrip	radial stubs at f_0, f_1	≈12 dBm*	37%
[64]'13	25.7	Dual-microstrip stubs	NA	NR	≈17%
[11]'92	35	microstrip λ/4 transformer	Tapered line and shunt stubs LPF	9.2	35%
[43]'16	35	Coplanar stripling	LPF and tapered DC terminals	≈8 dBm	60%
[52]'14	35	L-microstrip	LPF only	≈4 dBm	67%
[25]'15	94	Coplanar stripline	LPF only	<0 dBm*	37.7%

*Calculated from the PCE curve; NR: not reported

The layout of the rectifier is shown in Fig. 7-c. A dual-band voltage doubler rectifier was proposed in [42] based on dual-shunt stubs transmission line matching. The input impedance of the rectifier was evaluated after a transmission line gap between the matching network and the rectifier (Fig. 7-a), which was found to improve the PCE. The matching network was designed based on HB simulation in ADS.

A common feature among most rectifiers is the use of vias for single-series [23], self-biased [82], and voltage-doubler rectifiers [40], [42], [44]. However, for printed and flexible electronics, vias involve complicated fabrication processes and additional steps [24]. Thus, via-free rectifiers with single-sided current return paths have been proposed for single-ended microstrip-fed single-series rectifiers [24], [50], [87]. The current return path would typically include some form of harmonic termination such as radial stubs. The DC terminals of the rectifier are then both present on the top layer. For shunt diodes, the process is more straightforward as the positive and negative terminals of the rectifier are on the same layer [11], [43]. Fig. 7-c shows the layout of the shunt rectifier in [43] with no vias and a tapered line DC-pass filter on the DC terminals.

Although at mmWave bands beyond 60 GHz, the majority of implementations are based on fully-integrated CMOS devices (Table 4), Hemour *et al.* proposed the highest PCE rectenna at 94 GHz with over 3× PCE improvements over CMOS implementations [25]. Despite being implemented on a very low loss alumina substrate (alumina's 60 GHz $\tan\delta<0.001$ [88]), it was observed that the surface current losses peaked in the matching network [25]. The rectenna had an overall size of $0.55\lambda^2$ which, despite being larger than fully-integrated CMOS rectennas, is still usable for applications such as swarm micro-robotics. This is a particularly interesting example where a Schottky-based rectenna outperforms its CMOS counterparts, based on a diode with very low parasitics and V_F, on a very low-loss substrate.

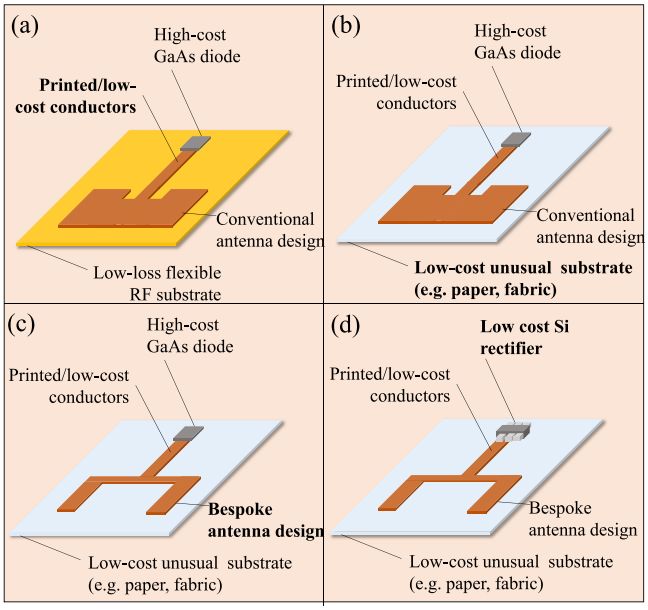

FIGURE 8. Low-cost mmWave rectenna categories: (a) low-cost conductors on flexible RF substrates [24], (b) low-cost conductors and substrate [49], (c) bespoke antenna design for high efficiency on lossy substrate [44], (d) the all low-cost components rectenna concept avoiding the use of costly mmWave GaAs diodes.

VII. ADDITIVE MANUFACTURING AND LOW-COST MMWAVE RECTENNAS

A. LOW-COST RECTENNA TOPOLOGIES AND MOTIVATION

A major driver for self-powered electronics and efficient energy transfer and distribution are low-cost IoT devices. Many of the mmWave rectenna implementations can be leveraged in space and defense applications, where the materials and diodes cost is negligible. However, for ubiquitous mmWave-powered networks to become a reality, several research challenges need to be overcome to allow high-efficiency low-cost rectennas. This section reviews the advances in additively-manufactured and flexible low-cost rectennas, as well as the viability of mmWave rectennas on lossy substrates. More broadly, low-cost and unusual mmWave antenna designs proposed for wireless communications are also reviewed based on their suitability for enabling new mmWave power harvesting applications.

To properly evaluate flexible and printed mmWave rectennas they need to be categorized based on their various components as in Fig. 8. The first class (Fig. 8-a) of flexible and conformable rectennas are those involving low-cost fabrication techniques to realize the rectenna on a flexible high frequency substrate. This substrate could be commercially available Liquid Crystal Polymer (LCP) which has $\tan\delta<0.005$. Various implementations have been presented using this fabrication method and all implementations were based on common geometry microstrip patch antennas [24], [50]. Such rectennas can achieve a DC output close to or surpassing their counterparts on rigid PCBs as in [74]. However, they cannot be classified as fully low-cost components as they still rely on expensive high-frequency

substrates which can be over 90× more expensive than fiberglass or plastics [89].

The second class of low-cost rectennas are those implemented on lossy conventional substrates (Fig. 8-b). Such implementations are more suited to real-life applications as their performance is not dependent on using low-loss substrates to realize complex impedance matching networks. For example, the rectenna in [49] is a demonstration of a mmWave-powered system-in-package. However, as the design is based on conventional antenna designs, the performance may be further improved through higher radiation efficiency antennas designed specifically for a lossy substrate.

The third class of low-cost rectennas is based on novel antenna design for maximizing the radiation efficiency on a lossy substrate (Fig. 8-c). The radiation efficiency in [44] was improved by over 3 dB compared to a microstrip patch on the same textile substrate due to the proposed antenna design. Nevertheless, the rectenna still employs a relatively costly GaAs diode which requires careful handling, encapsulation, and ESD protection [23].

The only fully low-cost mmWave topology not only employs bespoke antennas on low-cost substrates but also requires robust and low-cost rectifiers, as in Fig. 8-d. While Schottky diodes for mmWave applications will remain on GaAs to avoid operating near the cut-off frequency, the advances in CMOS mmWave rectifiers could be leveraged to realize low-cost printed rectennas. From a research and development perspective, the cost and time barrier of custom CMOS design for mmWave rectifiers contributes to the drive towards using off-the-shelf Schottky diodes, albeit being a costly component. However, for mass production, the high-efficiency rectifiers realized in standard CMOS processes could be used as the rectifying elements in future ubiquitous mmWave rectennas [86].

B. RECTENNA DESIGN, FABRICATION AND PERFORMANCE

A variety of fabrication techniques have been developed based on additive manufacturing, photolithography, and hybrid methods to realize flexible mmWave antennas and systems. For example, inkjet printing of antennas directly on flexible substrates using conductive inks is a straightforward process of printing multi-layered aperture coupled antennas using printable dielectrics [90]. Furthermore, inkjet masking has been used to deposit photoresistive inks to allow the etching of commercially-available polyimide copper laminates without the use of masks and precision mask aligners [91]. Fig. 9 shows photographs of mmWave rectennas fabricated using a variety of low-cost techniques such as printing on flexible and printed substrates.

As in Fig. 2 and in Table 2, the majority of mmWave rectennas were based on 50Ω antennas. Thus, flexible and printed antennas proposed for 5G and license-free communications beyond 24 GHz can be employed in mmWave power harvesting. Examples of flexible and printed antennas

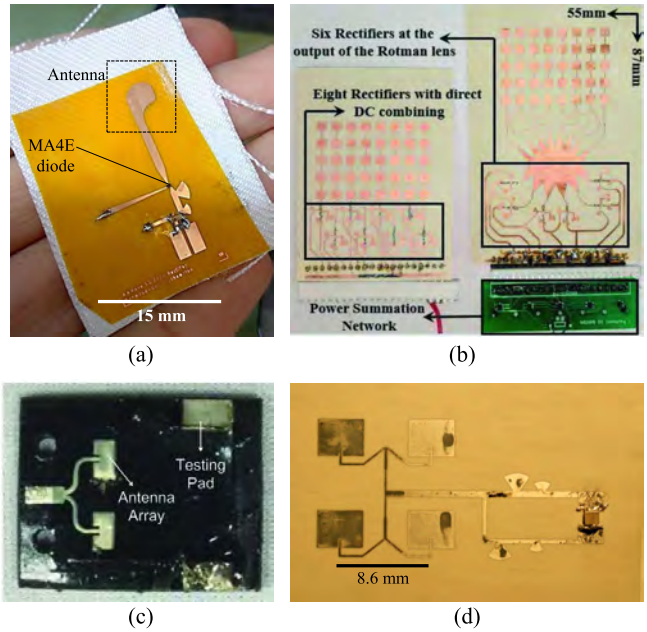

FIGURE 9. Photographs of flexible and printed mmWave rectennas: (a) textile broadband 20-26.5 GHz rectenna [44], (b) high gain and wide-beam inkjet-masked rectenna (reproduced from [50]), (c) 3D printed system-in-package rectenna (reproduced from [49]), (d) flexible inkjet-printed rectenna (reproduced from [24]).

developed for wireless communications have shown the possibility of achieving very high radiation efficiency (>80%) and a wide-bandwidth for 5G applications in [92]. Similarly, Body Area Network (BAN) flexible antennas have been demonstrated at 60 GHz based on flexible PCBs [93]. However, as for the LCP-based rectennas in [24], [50], these antennas were implemented on substrates with $\tan\delta < 0.005$. Hence, they cannot be considered as fully low-cost components and the designs may need to be optimized to achieve high radiation efficiencies on lossy substrates.

Eid *et al.* proposed flexible beamforming arrays based on Rotman lenses (Fig. 9-b) as an enabler of long range power harvesting [50] and backscattering [74]. The inkjet masking fabrication technique used, first presented in [91], is fairly low-cost and well-suited for rapid prototyping. However, the systems are implemented on low-loss Rogers LCP substrates. It is unclear how the performance of such a system, considering the complex Rotman lens, will vary if it was implemented on a lossy dielectric such as FR4, lossy polymers, or textiles. Considering only the microstrip feeds dielectric losses, based on the formulas in [94], the 55 mm-length microstrip rectenna feed will incur over 6 dB insertion losses at 28 GHz for a $\tan\delta = 0.02$. $\tan\delta = 0.02$ is a conservative estimate based on the properties of materials such as fabrics [41], [44] or 3D printable dielectrics [49], $\tan\delta$ of substrates such as paper can exceed 0.04 [95]. It is expected that the dielectric losses will be also higher in the Rotman lens due to the unusual geometry and the larger area over a lossy dielectric. Similar conclusions could be drawn on rectenna arrays printed or etched on flexible low-loss substrates such as [24],

where the net DC output will degrade significantly should the system be transferred to a lossy substrate.

A particularly common example of antenna substrates which have a high tanδ are textiles. Driven and parasitic mmWave antenna arrays have been recently presented as high as 77 GHz with 11.2 dB gain [96]. mmWave antennas on textiles have also been developed for on/off-body BAN applications [41], [97]. The only rectenna implementation on textiles was presented in [44] and suffered from lower PCE compared to rectennas using the same diode. From an antenna perspective, the radiation efficiency of mmWave textile antennas varied between 48% at 60 GHz in [41] to 77% at 24 GHz in [44]. Considering the 41% efficiency patch array in [41] and the end-fire 48% quasi-Yagi in [97], meaningful conclusions can be drawn upon the effect of the antenna design on a lossy substrate at mmWave bands can be drawn. Both antennas, by Chahat *et al.* have been fabricated using the same conductors and on the same cotton substrate by the same group. Yet, the endfire antenna achieves over 1 dB higher efficiency. In [44], the reflector-backed antipodal Vivaldi antenna achieved more than 3 dB higher radiation efficiency and gain compared to a microstrip patch operating at the same frequency and on the same textile substrate. This highlights the significance of a different antenna design methodology specifically aimed towards lossy substrates.

Table 6 compares the recent flexible and low-cost rectifiers' performance. The rectifier in [50] achieve the highest PCE of ≈33%, only 21% lower than the high efficiency rectenna implemented on a rigid PCB in [23]. Reference [50] uses a solid metal sheet for the antenna and the ground plane to improve the conductivity above 20 GHz. Thus, as discussed in Section VII-A, such implementations are on low-loss substrates and can hence achieve a high PCE using optimal matching network design. Yet, it is hard to verify this assumption as the rectifier's S_{11} is not reported for any of the rectennas compared in Table 6 with the exception of [44].

Comparing [44] and [49]: the two rectennas implemented on lossy substrates (3D printed substrate and textiles, respectively), both rectennas achieve relatively low PCEs. Nevertheless, the low PCEs are not directly a function of the material-induced losses. For instance, both designs prioritized high voltage sensitivity by using a high impedance load to demonstrate the feasibility of turning on low power electronics. In addition, the rectenna in [44] is designed for broadband operation and the rectifier has a high S_{11} due to the constraints on the matching network design. Therefore, it can be concluded that there is a potential for a high PCE rectenna low-cost lossy materials. However, the past implementations were either oriented towards improving the voltage sensitivity or bandwidth and hence did not have the optimum PCE.

Studies focusing only on the simulated performance of printed rectifiers have also been proposed. In [98], the performance of a rectenna based on a paper substrate (tan$\delta = 0.045$) was simulated showing the potential of up to 35.2% at 15 dBm. Despite showing a fabricated prototype, no measurement results of the PCE were presented, which illustrates the difficulty of achieving reliable interconnects at mmWave bands both for mounting components and for interfacing with lab instrumentation. In [87], a ramp interconnect based on printed dielectrics and conductors was proposed to attach the W-band diode ZBD to a flexible substrate. However, as pointed out in the discussion of Fig. 8, high frequency GaAs Schottky diodes such as the ZBD are not low cost components. As with [98], no experimental results of the proposed rectifier were presented.

TABLE 6. Comparison of printed and flexible mmWave rectifiers.

Lit.	Frequency (GHz)	Rectifier S_{11}	10 dBm DC V. at Z-Load	Max PCE
[24]'17	24	NR	0.8 V@739Ω	7.6%
[50]'19	28	NR	1.4 V@1kΩ	30%
[49]'19	28	NR	0.7 V@750kΩ	<1%
[44]'20	20-26.5	−2 dB	1.3 V@10kΩ	8.5%

VIII. FUTURE ANTENNA DESIGN CHALLENGES

To bring mmWave rectennas and wireless power harvesting to mainstream use and ubiquitous IoT devices, several research challenges exist in the topic of antenna and rectenna design. In this section, a selection of recent mmWave antenna research efforts is reviewed highlighting their applicability to power harvesting in future IoT networks.

The challenge of realizing low-cost rectennas was partially addressed using additive manufacturing, as reviewed in Section VII, where a variety of high-performance rectennas such as [50] were demonstrated on flexible substrates. 3D and functional material printing can be further explored to improve the implementation of mmWave WPT systems. Recent work in [99] has shown the possibility to 3D and inkjet print a functional transmitter "PCB" on top of a compact 3D printed horn antenna, presenting a "System on Antenna" (SoA) [99]. The SoA operating at 15 GHz shows the potential to extend this concept to mmWave bands in the 24-40 GHz range. Such a concept could be adapted to realize rectenna-powered systems on additively-manufactured horn antennas, where the printed microstrip rectifier can connect to the horn using a low-cost printed microstrip to waveguide transition. A 3D-printed horn-based SoA can significantly reduce the costs and manufacturing time of waveguide rectennas, such as [53], while maintaining the desired radiation properties. The SoA concept also shows potential for being used as a low-cost mmWave-ID reader which allows interfacing with the tags and antennas proposed in [48], [100], [101]. A mmWave-ID reader would be more compact compared to existing sub-1 GHz readers while maintaining high gain.

Similar to integrating microwave components in 3D printed antennas, functional transmitters and power amplifiers have been impregnated in textiles [102]. Given the advances in textile-based mmWave antennas, [41], [97], [103], and systems, [44], [96],

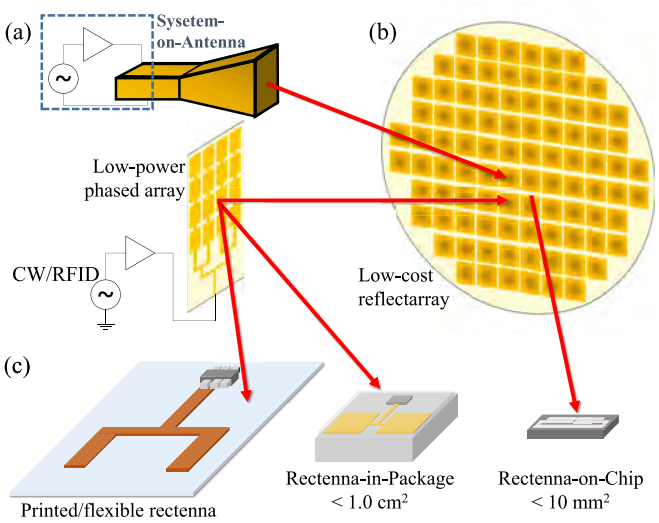

FIGURE 10. Future mmWave-powered concept: (a) Directional transmitter based on printed high-gain SoA or phased array, (b) reflectarray for redirecting power, (c) mmWave rectennas in different processes and scales.

"Pregtronics", i.e., RF components impregnated in conductive textiles, can be extended to mmWave bands [102].

In addition to 3D printed SoAs, a fully 3D-printable high gain reflectarray was proposed in [104]. The use of such low-cost reflectarrays can improve the angular coverage of both mmWave rectennas and WPT antennas. The natural existence of reflectors such as lamp-posts and vehicles was found to improve the mmWave link in urban environments [105]. Subsequently, deployment of low-cost reflectarrays can improve the WPT links over longer ranges for N-LoS links.

Minimizing the size of rectifiers is an open research challenge which hinders the adoption of mmWave rectennas. Schottky-based rectifiers such as [40], [43] occupy significant board area compared to the antenna, due to the harmonics-termination or LPF. Thus, the area of mmWave rectennas, e.g., [23], [51], has been larger than rectennas operating as low as 2.4 GHz [38], which can harvest significantly higher DC power from μW/cm^2 power densities while being implemented on low-cost substrates [38]. Therefore, research in minimizing the area of mmWave rectifiers, and investigating the trade-offs between the rectifier's area and the achievable PCE is needed to justify the potential miniaturization in the antenna. The majority of rectenna implementations included long microstrip feedlines connecting the "compact" antennas with the rectifiers which results in an overall larger system [23], [43], [44]. Rectifier minimization will enable the adoption of compact antenna designs such as antennas-in-package [106], and dielectric resonator antennas, to be used for mmWave power harvesting.

Integration of CMOS rectifiers with off-chip antennas has not been widely presented at mmWave bands yet. As an off-chip dielectric resonator was used to realize the dual-band mm-ID antenna in [48], additional off-chip components such as parasitic patch radiators and multi-layered antennas can be used to enhance fully-integrated rectennas' gain [107]. 3D antenna stacking could be applied to realize fully-integrated rectennas with antennas-in-package with significantly higher gain and radiation efficiency than the fully-integrated CMOS antennas in [47], [56]. The off-chip artificial magnetic conductor in [107] was used to improve an on-chip monopole antenna gain by 20 dB. Such improvement could translate to extending the operation range of a mmWave rectenna by over 10×.

As for antennas-in-package (AiP), considering the multi-beam AiP proposed for 57-66 GHz RFICs in [108], the boresight and broadside gains of 5 and 6.3 dB, respectively, can significantly improve the efficient harvesting range of rectifiers such as [109] compared to an on-chip antenna such as [56]. Multi-directional radiation patterns similar to those achieved by the AiP in [108] have been used to improve the power harvesting capabilities of ambient RF energy harvesting rectennas at sub-6 GHz bands [73]. Mutli-beam rectennas are particularly relevant at mmWave bands to allow for high-gain yet quasi-omnidirectional power harvesting.

Beamforming antenna arrays for rectennas are expected to attract significant interest. For instance, the LCP patch rectenna array in [50] based on the Rotman beamforming lens achieves a longer operation range than other harvesters operating at the same frequency. Furthermore, the use of a similar beamforming patch array was demonstrated in [74] for long-range retro-directive backscatter communications for RFID applications at 28 GHz. Given the 75 dBm EIRP of 5G systems, the beamforming tag would have a read-range of 1.8 km. Such range is not matched by UHF RFID systems and demonstrates the benefits of mmWave power harvesting and passive wireless communications. The practical demonstration with a 48 dBm EIRP in [74] shows a very long tag read-range of 64 m, which exceeds conventional UHF RFID which is often around 20 m. Although the RFID Rotman-lens array backscatter modulator was powered using a flexible solar cell [74], given its low power consumption of 2.64 μW it can be powered using a rectenna based on the same Rotman lens, similar to the implementation in [50]. Therefore, integration of rectennas with backscattering modulators based on shared antenna arrays will be a promising area for mmWave power harvesting where beamforming networks outperform single-direction mmWave-ID Van Atta arrays such as [110], [111], in terms of angular coverage.

Combining the reviewed advances in mmWave antennas, rectifiers, and intermediate reflectors, a mmWave-powered network shown in Fig. 10 can power a high density of miniaturized edge nodes fabricated using various processes. The optimized mmWave link will allow low interference, high end-to-end efficiency and improved energy coverage, which have all been identified as advantages of mmWave power harvesting over traditional UHF bands [27]. Such a concept will enable mmWave bands to become an integral part of future

IoT networks not only for high data-rate communications but also for power transmission.

IX. CONCLUSION

The mmWave bands represent an emerging platform for wireless power transmission and harvesting. The advances in mmWave power transmission since the 1990s combined with recent advances in 5G mmWave hardware present mmWave power harvesting as an enabler of future wireless-powered networks. This article has presented a comprehensive review of the recent advances in mmWave rectenna design and the broader advances in antennas, propagation, and rectifiers which can be leveraged for efficient wireless powered networks at mmWave bands.

The requirements and challenges for efficient power transmission and harvesting have been reviewed for individual system components. The key requirements for efficient mmWave power transmission may be summarized as:

1) Efficient high gain antenna and array designs not limited to low-loss RF substrates.
2) Impedance matched, high sensitivity and PCE rectifiers, based on accurate diode and package models, enabling rapid design and simulations.
3) Antenna-rectifier fabrication and packaging techniques to allow reliable and scalable integration of high-$f_{\text{cut}-\text{off}}$ Schottky or CMOS rectifiers with high-gain low-cost antennas.

Holistic design of mmWave rectennas involving both antenna and rectifier co-design based on low-cost semiconductors and packaging techniques will be needed for reliable high-efficiency harvesters. Finally, research into novel antenna-in-package and printed antenna designs combined with integrated CMOS system will be crucial to enable wide-scale pervasive adoption of mmWave-powered systems.

ACKNOWLEDGMENT

The authors would like to thank Dr. C. R. Valenta from Georgia Tech Research Institute for giving permission to reuse the MATLAB code used in the rectifier analysis. Datasets used in this article are accessible from the University of Southampton repository at doi: 10.5258/SOTON/D1568.

REFERENCES

[1] X. Lu, P. Wang, D. Niyato, D. I. Kim, and Z. Han, "Wireless networks with RF energy harvesting: A contemporary survey," *IEEE Commun. Surveys Tuts.*, vol. 17, no. 2, pp. 757–789, 2nd Quart., 2015.

[2] J. Charthad, N. Dolatsha, A. Rekhi, and A. Arbabian, "System-level analysis of far-field radio frequency power delivery for mm-sized sensor nodes," *IEEE Trans. Circuits Syst.*, vol. 63 no. 2, pp. 300–311, Nov. 2016.

[3] C. Yuan, Y. Deng, T. Li, and F. Yang, "Manufacturing energy analysis of lithium ion battery pack for electric vehicles," *CIRP Ann.*, vol. 66, no. 1, pp. 53–56, 2017.

[4] C. R. Valenta and G. D. Durgin, "Harvesting wireless power: Survey of energy-harvester conversion efficiency in far-field, wireless power transfer systems," *IEEE Microw. Mag.*, vol. 15, no. 4, pp. 108–120, May 2014.

[5] T. Soyata, L. Copeland, and W. Heinzelman, "RF energy harvesting for embedded systems: A survey of tradeoffs and methodology," *IEEE Circuits Syst. Mag.*, vol. 16, no. 1, pp. 22–57, Feb. 2016.

[6] U. Guler and M. Ghovanloo, "Power management in wireless power-sipping devices: A survey," *IEEE Circuits Syst. Mag.*, vol. 17, no. 4, pp. 64–82, Nov. 2015.

[7] M. Shanawani, D. Masotti, and A. Costanzo, "THz rectennas and their design rules," *Electronics*, vol. 6, no. 4, p. 99, 2017.

[8] S. K. Divakaran, D. D. Krishna, and Nasimuddin, "RF energy harvesting systems: An overview and design issues," *Int. J. RF Microw. Comput.-Aided Eng.*, vol. 29, no. 1, pp. 43–55, 2018.

[9] M. Cansiza, D. Altinel, and G. K. Kurt, "Efficiency in RF energy harvesting systems: A comprehensive review," *Energy*, vol. 174, pp. 292–309, May 2019.

[10] M. Wagih, A. S. Weddell, and S. Beeby, "Rectennas for RF energy harvesting and wireless power transfer: A review of antenna design [antenna applications corner]," *IEEE Antennas Propag. Mag.*, vol. 62 no. 5, pp. 119–123, May 2020.

[11] T.-W. Yoo and K. Chang, "Theoretical and experimental development of 10 and 35 GHz rectennas," *IEEE Trans. Mirow Theory Techn.*, vol. 40, no. 6, pp. 1259–1266, Jul. 1992.

[12] P. Koert and J. Cha, "Millimeter wave technology for space power beaming," *IEEE Trans. Mirow Theory Techn.*, vol. 40 no. 6, pp. 1251–1258, Jul. 1992.

[13] M. Pinuela, P. D. Mitcheson, and S. Lucyszyn, "Ambient RF energy harvesting in urban and semi-urban environments," *IEEE Trans. Microw. Theory Techn.*, vol. 61, no. 7, pp. 2715–2726, May 2013.

[14] C. Song, Y. Huang, J. Zhou, J. Zhang, S. Yuan, and P. Carter, "A high-efficiency broadband rectenna for ambient wireless energy harvesting," *IEEE Trans. Antennas Propag.*, vol. 63, no. 8, pp. 3486–3495, May 2015.

[15] C. Song *et al.*, "A novel six-band dual CP rectenna using improved impedance matching technique for ambient RF energy harvesting," *IEEE Trans. Antennas Propag.*, vol. 64, no. 7, pp. 3160–3171, May 2016.

[16] H. J. Visser and R. J. M. Vullers, "RF energy harvesting and transport for wireless sensor network applications: Principles and requirements," *Proc. IEEE*, vol. 101, no. 6, pp. 1410–1423, Apr. 2013.

[17] S. A. Nauroze *et al.*, "Additively manufactured RF components and modules: Toward empowering the birth of cost-efficient dense and ubiquitous IoT implementations," *Proc. IEEE*, vol. 105, no. 4, pp. 702–722, Feb. 2017.

[18] S. Kim *et al.*, "Ambient RF energy-harvesting technologies for self-sustainable standalone wireless sensor platforms," *Proc. IEEE*, vol. 102, no. 11, pp. 1649–1666, Nov. 2014.

[19] W. Brown, "The history of power transmission by radio waves," *IEEE Trans. Microw. Theory Techn.*, vol. MTT-32, no. 9, pp. 1230–1242, Sep. 1984.

[20] T. Yoo and K. Chang, "35 GHz integrated circuit rectifying antenna with 33 efficiency," *Electron. Lett.*, vol. 27 no. 23, p. 2117, 1992.

[21] P. Koert and J. Cha, "35 and 94 GHz rectifying antenna systems," in *Proc. 2nd Int. Symp. Power Space (SPS)*, 1991, pp. 1–9.

[22] P. Bailey and N. Worthington, "History and applications of haarp technologies: The high frequency active auroral research program," in *Proc. 32nd Intersoc. Energy Convers. Eng. Conf. (IECEC)*, 1997, p. 208.

[23] S. Ladan, A. B. Guntupalli, and K. Wu, "A high-efficiency 24 GHz rectenna development towards millimeter-wave energy harvesting and wireless power transmission," *IEEE Trans. Circuits Syst.*, vol. 61, no. 12, pp. 3358–3366, Aug. 2014.

[24] J. Bito *et al.*, "Millimeter-wave ink-jet printed RF energy harvester for next generation flexible electronics," in *Proc. IEEE Wireless Power Transf. Conf. (WPTC)*, 2017, pp. 1–4.

[25] S. Hemour, C. H. P. Lorenz, and K. Wu, "Small-footprint wideband 94 GHz rectifier for swarm micro-robotics," in *Proc. IEEE MTT-S Int. Microw. Symp.*, 2015, pp. 1–3.

[26] G. Nikandish, R. B. Staszewski, and A. Zhu, "Breaking the bandwidth limit: A review of broadband doherty power amplifier design for 5G," *IEEE Microw. Mag.*, vol. 21, no. 4, pp. 57–75, Mar. 2020.

[27] T. A. Khan, A. Alkhateeb, and R. W. Heath, "Millimeter wave energy harvesting," *IEEE Trans. Wireless Commun.*, vol. 15, no. 9, pp. 6048–6062, Sep. 2016.

[28] B. Clerckx, A. Costanzo, A. Georgiadis, and N. B. Carvalho, "Wireless power transmission: From far field to near field," *IEEE Microw. Mag.*, vol. 19, no. 6, pp. 69–82, Apr. 2018.

[29] H. Kazemi, K. Shinohara, and C. W. Eckhardt, "Millimeter wave wireless power transmission-technologies and applications," in *Proc. IEEE Wireless Power Transf. Conf.*, 2019, pp. 1–4.

[30] C. Balanis, *Antenna Theory: Analysis and Design*. Hoboken, NJ, USA: Wiley, 2005, pp. 92–94.

[31] I. A. Hemadeh, K. Satyanarayana, M. El-Hajjar, and L. Hanzo, "Millimeter-wave communications: Physical channel models, design considerations, antenna constructions, and link-budget," *IEEE Commun. Surveys Tuts.*, vol. 20, no. 2, pp. 870–913, 3rd Quart., 2017.

[32] S. Salous *et al.*, "Millimeter-wave propagation: Characterization and modeling toward fifth-generation systems. [wireless corner]," *IEEE Antennas Propag. Mag.*, vol. 58 no. 6, pp. 115–127, Dec. 2016.

[33] S.-E. Adami *et al.*, "A flexible 2.45-GHz power harvesting wristband with net system output from −24.3 dBm of RF power," *IEEE Trans. Microw. Theory Techn.*, vol. 66 no. 1, pp. 380–395, May 2018.

[34] Y.-S. Chen and C.-W. Chiu, "Maximum achievable power conversion efficiency obtained through an optimized rectenna structure for RF energy harvesting," *IEEE Trans. Antennas Propag.*, vol. 65, no. 5, pp. 2305–2317, Mar. 2017.

[35] M. Wagih, A. S. Weddell, and S. Beeby, "High-efficiency sub-1 GHz flexible compact rectenna based on parametric antenna-rectifier co-design," in *Proc. IEEE MTT-S Int. Microw. Symp.*, 2020, pp. 1–6.

[36] H. Sun, Y. X. Guo, M. He, and Z. Zhong, "A dual-band rectenna using broadband Yagi antenna array for ambient RF power harvesting," *IEEE Antennas Wireless Propag. Lett.*, vol. 12, pp. 918–921, 2013.

[37] H. J. Visser, S. Keyrouz, and A. B. Smolders, "Optimized rectenna design," *Wireless Power Transf.*, vol. 2, no. 1, pp. 44–50, 2017.

[38] C. Domnik, S. Husges, and C. Degen, "Frugal energy harvesting: Microwave energy radiated into the environment from wireless networks," *IEEE Microw. Mag.*, vol. 9, no. 5, pp. 454–462, Nov. 2014.

[39] C. Song *et al.*, "Matching network elimination in broadband rectennas for high-efficiency wireless power transfer and energy harvesting," *IEEE Trans. Ind. Electron.*, vol. 64, no. 5, pp. 3950–3961, Mar. 2017.

[40] S. Ladan and K. Wu, "Nonlinear modeling and harmonic recycling of millimeter-wave rectifier circuit," *IEEE Trans. Microw. Theory Techn.*, vol. 63, no. 3, pp. 937–944, Jan. 2015.

[41] N. Chahat, M. Zhadobov, S. A. Muhammad, L. L. Coq, and R. Sauleau, "60-GHz textile antenna array for body-centric communications," *IEEE Trans. Antennas Propag.*, vol. 61 no. 4, pp. 1816–1824, Apr. 2013.

[42] A. Riaz, M. Awais, M. M. Farooq, and W. T. Khan, "A single cell dual band rectifier at millimeter-wave frequencies for future 5G communications," in *Proc. 49th Eur. Microw. Conf. (EuMC)*, 2019, pp. 1–3.

[43] M. Bozzi, A. Georgiadis, and K. Wu, "High-efficiency microstrip rectenna for microwave power transmission at Ka band with low cost," *IET Microw. Antennas Propag.*, vol. 10 no. 15, pp. 1648–1655, 2016.

[44] M. Wagih, G. S. Hilton, A. S. Weddell, and S. Beeby, "Broadband millimetre-wave textile-based flexible rectenna for wearable energy harvesting," *IEEE Trans. Microw. Theory Techn.*, early access, Sep. 4, 2020, doi: 10.1109/TMTT.2020.3018735.

[45] A. Takacs, H. Aubert, S. Fredon, L. Despoisse, and H. Blondeaux, "Microwave power harvesting for satellite health monitoring," *IEEE Trans. Microw. Theory Techn.*, vol. 62, no. 4, pp. 1090–1098, Feb. 2014.

[46] S. Ladan, "Simultaneous wireless power transmission and data communication," Ph.D. dissertation, Université de Montréal, Montreal, QC, Canada, 2014.

[47] M. Tabesh, N. Dolatsha, A. Arbabian, and A. M. Niknejad, "A power-harvesting pad-less millimeter-sized radio," *IEEE J. Solid-State Circuits*, vol. 50, no. 4, pp. 962–977, Mar. 2015.

[48] P. Burasa, T. Djerafi, N. G. Constantin, and K. Wu, "On-chip dual-band rectangular slot antenna for single-chip millimeter-wave identification tag in standard CMOS technology," *IEEE Trans. Antennas Propag.*, vol. 65, no. 8, pp. 3858–3868, May 2017.

[49] T.-H. Lin, S. N. Daskalakis, A. Georgiadis, and M. M. Tentzeris, "Achieving fully autonomous system-on-package designs: An embedded-on-package 5G energy harvester within 3D printed multilayer flexible packaging structures," in *Proc. IEEE MTT-S Int. Microw. Symp. (IMS)*, 2019, pp. 1375–1378.

[50] A. Eid, J. Hester, and M. M. Tentzeris, "A scalable high-gain and large-beamwidth mm-Wave harvesting approach for 5G-powered IoT," in *Proc. IEEE MTT-S Int. Microw. Symp. (IMS)*, 2019, pp. 1309–1312.

[51] B. T. Malik *et al.*, "Wireless power transfer system for battery-less sensor nodes," *IEEE Access*, vol. 8, pp. 95878–95887, 2020.

[52] A. Mavaddat, S. H. M. Armaki, and A. R. Erfanian, "Millimeter-wave energy harvesting using 4×4 microstrip patch antenna array," *IEEE Antennas Wireless Propag. Lett.*, vol. 14, pp. 515–518, 2014.

[53] Q. Chen, Z. Liu, Y. Cui, H. Cai, and X. Chen, "A metallic waveguide-integrated 35-GHz rectenna with high conversion efficiency," *IEEE Microw. Wireless Compon. Lett.*, vol. 30, no. 8, pp. 821–824, Aug. 2020, doi: 10.1109/LMWC.2020.3002163.

[54] M. Nariman, F. Shirinfar, A. P. Toda, S. Pamarti, A. Rofougaran, and F. D. Flaviis, "A compact 60-GHz wireless power transfer system," *IEEE Trans. Microw. Theory Techn.*, vol. 64, no. 8, pp. 2664–2677, Jul. 2016.

[55] C. Hannachi, S. Boumaiza, and S. O. Tatu, "A highly sensitive broadband rectenna for low power millimeter-wave energy harvesting applications," in *Proc. IEEE Wireless Power Transf. Conf. (WPTC)*, 2018, pp. 1–4.

[56] H. Gao *et al.*, "A 71GHz RF energy harvesting tag with 8% efficiency for wireless temperature sensors in 65nm CMOS," in *Proc. IEEE Radio Freq. Integr. Circuits Symp. (RFIC)*, 2013, pp. 403–406.

[57] K. Matsui *et al.*, "Development of 94GHz microstrip line rectenna," in *Proc. IEEE Wireless Power Transf. Conf. (WPTC)*, 2018, pp. 1–4.

[58] N. Weissman, S. Jameson, and E. Socher, "W-band CMOS on-chip energy harvester and rectenna," in *Proc. IEEE MTT-S Int. Microw. Symp. (IMS)*, 2014, pp. 1–3.

[59] E. Lier, "Review of soft and hard horn antennas, including metamaterial-based hybrid-mode horns," *IEEE Antennas Propag. Mag.*, vol. 52 no. 2, pp. 31–39, Jul. 2018.

[60] Y.-J. Ren and K. Chang, "5.8-GHz circularly polarized dual-diode rectenna and rectenna array for microwave power transmission," *IEEE Trans. Microw. Theory Techn.*, vol. 54 no. 4, pp. 1495–1502, Apr. 2006.

[61] D. M. Pozar, "Microstrip antennas," *Proc. IEEE*, vol. 80 no. 1, pp. 79–91, May 1992.

[62] M. Bozzi, A. Georgiadis, and K. Wu, "Review of substrate-integrated waveguide circuits and antennas," *IET Microw. Antennas Propag.*, vol. 5, no. 8, pp. 909–920, 2011.

[63] L. Yan, W. Hong, G. Hua, J. Chen, K. Wu, and T. J. Cui, "Simulation and experiment on SIW slot array antennas," *IEEE Microw. Compon. Lett.*, vol. 14, no. 9, pp. 446–448, Sep. 2004.

[64] A. Collado and A. Georgiadis, "24 GHz substrate integrated waveguide (SIW) rectenna for energy harvesting and wireless power transmission," in *Proc. IEEE MTT-S Int. Microw. Symp. Dig. (MTT)*, 2013, pp. 1–4.

[65] G.-N. Tan, X.-X. Yang, H. Mei, and Z.-L. Lu, "Study on millimeter-wave vivaldi rectenna and arrays with high conversion efficiency," *Int. J. Antennas Propag.*, vol. 2016, 2016, Art. no. 1897283.

[66] R. Moro, S. Agneessens, H. Rogier, A. Dierck, and M. Bozzi, "Textile microwave components in substrate integrated waveguide technology," *IEEE Trans. Microw. Theory Techn.*, vol. 63, no. 2, pp. 422–432, Sep. 2015.

[67] L. Alonso-Gonzalez, S. Ver-Hoeye, C. Vazquez-Antuna, M. Fernandez-Garcia, and F. L.-H. Andres, "On the techniques to develop millimeter-wave textile integrated waveguides using rigid warp threads," *IEEE Trans. Microw. Theory Techn.*, vol. 66, no. 2, pp. 751–761, Apr. 2018.

[68] Y. P. Zhang and D. Liu, "Antenna-on-chip and antenna-in-package solutions to highly integrated millimeter-wave devices for wireless communications," *IEEE Trans. Antennas Propag.*, vol. 57, no. 10, pp. 2830–2841, Apr. 2009.

[69] H. Dagan *et al.*, "A low-power low-cost 24 GHz RFID tag with a C-flash based embedded memory," *IEEE J. Solid-State Circuits*, vol. 49 no. 9, pp. 1942–1957, Mar. 2014.

[70] H.-K. Chiou and I.-S. Chen, "High-efficiency dual-band on-chip rectenna for 35- and 94-GHz wireless power transmission in 0.13-μm CMOS technology," *IEEE Trans. Microw. Theory Techn.*, vol. 58, no. 12, pp. 3598–3606, Oct. 2010.

[71] R. Garg and A. S. Natarajan, "A 28-GHz low-power phased-array receiver front-end with 360 RTPS phase shift range," *IEEE Trans. Microw. Theory Techn.*, vol. 65 no. 11, pp. 4703–4714, Sep. 2017.

[72] S. Lim and T. Itoh, "60-GHz retrodirective array system with efficient power management," in *Proc. Eur. Microw. Conf.*, 2006, pp. 314–317.

[73] E. Vandelle, D. H. N. Bui, T.-P. Vuong, G. Ardila, K. Wu, and S. Hemour, "Harvesting ambient RF energy efficiently with optimal angular coverage," *IEEE Trans. Antennas Propag.*, vol. 67, no. 3, pp. 1862–1873, Dec. 2019.

[74] A. Eid, J. Hester, and E. M. Tentzeris, "Rotman lens-based wide angular coverage and high gain semi-passive architecture for ultra-long range mm-Wave RFIDs," *IEEE Antennas Wireless Propag. Lett.*, early access, Jun. 16, 2020, doi: 10.1109/LAWP.2020.3002924.

[75] C. R. Valenta and G. D. Durgin, "Rectenna performance under power-optimized waveform excitation," in *Proc. IEEE Int. Conf. RFID (RFID)*, 2013, pp. 237–244.

[76] C. R. Valenta, M. M. Morys, and G. D. Durgin, "Theoretical energy-conversion efficiency for energy-harvesting circuits under power-optimized waveform excitation," *IEEE Trans. Microw. Theory Techn.*, vol. 63 no. 5, pp. 1758–1767, Aug. 2015.

[77] C. R. Valenta, "Microwave-energy harvesting at 5.8 GHz for passive devices," Ph.D. dissertation, Georgia Inst. Technol., Atlanta, GA, USA.

[78] C. A. Balanis, *Antenna Theory: Analysis and Design*. Hoboken, NJ, USA: Wiley-Intersci., 1982, pp. 98–100.

[79] J. Semple, D. G. Georgiadou, G. Wyatt-Moon, G. Gelinck, and T. D. Anthopoulos, "Flexible diodes for radio frequency (RF) electronics: A materials perspective," *Semicond. Sci. Technol.*, vol. 32, no. 12, 2017, Art. no. 123002.

[80] M. K. Matters-Kammerer, L. Tripodi, R. van Langevelde, J. Cumana, and R. H. Jansen, "RF characterization of schottky diodes in 65-nm CMOS," *IEEE Trans. Electron Devices*, vol. 57 no. 5, pp. 1063–1068, May 2010.

[81] B. Kapilevich *et al.*, "W-band rectenna coupled with low-barrier mott diode," *IEEE Microw. Wireless Compon. Lett.*, vol. 26 no. 8, pp. 637–639, Apr. 2016.

[82] S. Ladan, S. Hemour, and K. Wu, "Towards millimeter-wave high-efficiency rectification for wireless energy harvesting," in *Proc. IEEE Int. Wireless Symp. (IWS)*, 2013, pp. 1–6.

[83] C. H. P. Lorenz *et al.*, "Breaking the efficiency barrier for ambient microwave power harvesting with heterojunction backward tunnel diodes," *IEEE Trans. Microw. Theory Techn.*, vol. 63, no. 12, pp. 4544–4555, Apr. 2015.

[84] M. Yasir *et al.*, "Integration of antenna array and self-switching graphene diode for detection at 28 GHz," *IEEE Electron Device Lett.*, vol. 40, no. 4, pp. 628–631, Oct. 2019.

[85] H. Gao, D. M. Leenaerts, and P. Baltus, "A 62 GHz inductor-peaked rectifier with 7% efficiency," in *Proc. IEEE Radio Freq. Integr. Circuits Symp. (RFIC)*, 2013, pp. 189–192.

[86] H. Gao, M. Matters-Kammerer, D. Milosevic, and P. G. M. Baltus, *Batteryless mm-Wave Wireless Sensors*. Heidelberg, Germany: Springer, 2018.

[87] B. T. Malik, V. Doychinov, S. A. R. Zaidi, I. D. Robertson, N. Somjit, and R. Richardson, "Flexible rectennas for wireless power transfer to wearable sensors at 24 GHz," in *Proc. Res. Invent. Innov. Congr.*, 2019, pp. 1–9.

[88] D. D. Marco *et al.*, "Dielectric properties of pure alumina from 8 GHz to 73 GHz," *J. Eur. Ceramic Soc.*, vol. 36, pp. 3355–3361, May 2016.

[89] E. Shi, E. Centeno, R. Figueroa, C. Qi, and G. Durgin, "A rectenna using copper foil on glass to reduce cost of space solar power," in *Proc. IEEE Wireless Power Transf. Conf. (WPTC)*, 2019, pp. 421–425.

[90] B. S. Cook, B. Tehrani, J. R. Cooper, and M. M. Tentzeris, "Multilayer inkjet printing of millimeter-wave proximity-fed patch arrays on flexible substrates," *IEEE Antennas Wireless Propag. Lett.*, vol. 12, pp. 1351–1354, 2013.

[91] J. Bito, J. G. Hester, and M. M. Tentzeris, "Ambient RF energy harvesting from a two-way talk radio for flexible wearable wireless sensor devices utilizing inkjet printing technologies," *IEEE Trans. Microw. Theory Techn.*, vol. 63, 12, pp. 4533–4543, Apr. 2015.

[92] S. F. Jilani, M. O. Munoz, Q. H. Abbasi, and A. Alomainy, "Millimeter-wave liquid crystal polymer based conformal antenna array for 5G applications," *IEEE Antennas Wireless Propag. Lett.*, vol. 18, no. 1, pp. 84–88, Mar. 2019.

[93] M. Ur-Rehman, N. A. Malik, X. Yang, Q. H. Abbasi, Z. Zhang, and N. Zhao, "A low profile antenna for millimeter-wave body-centric applications," *IEEE Trans. Antennas Propag.*, vol. 65 no. 12, pp. 6329–6337, Jun. 2017.

[94] R. Hoffman, *Handbook of Microwave Integrated Circuits*. London, U.K.: Artech House, 1987.

[95] V. Palazzi *et al.*, "A novel ultra-lightweight multiband rectenna on paper for RF energy harvesting in the next generation LTE bands," *IEEE Trans. Microw. Theory Techn.*, vol. 66, no. 1, pp. 366–379, Jul. 2018.

[96] A. Meredov, K. Klionovski, and A. Shamim, "Screen-printed, flexible, parasitic beam-switching millimeter-wave antenna array for wearable applications," *IEEE Open J. Antennas Propag.*, vol. 1, pp. 2–10, 2020.

[97] N. Chahat, M. Zhadobov, L. L. Coq, and R. Sauleau, "Wearable endfire textile antenna for on-body communications at 60 GHz," *IEEE Antennas Wireless Propag. Lett.*, vol. 11, pp. 799–802, 2012.

[98] S. Daskalakis, J. Kimionis, J. Hester, A. Collado, M. M. Tentzeris, and A. Georgiadis, "Inkjet printed 24 GHz rectenna on paper for millimeter wave identification and wireless power transfer applications," in *Proc. IEEE MTT-S Int. Microw. Workshop Adv. Mater. Process. RF THz Appl. (IMWS-AMP)*, 2017, pp. 1–3.

[99] X. He, Y. Fang, R. A. Bahr, and M. M. Tentzeris, "RF systems on antenna (SoA): A novel integration approach enabled by additive manufacturing," in *Proc. IEEE MTT-S Int. Microw. Symp.*, 2020, pp. 1522–1525.

[100] P. Burasa, N. G. Constantin, and K. Wu, "High-efficiency wideband rectifier for single-chip batteryless active millimeter-wave identification (MMID) tag in 65-nm bulk CMOS technology," *IEEE Trans. Microw. Theory Techn.*, vol. 62, no. 4, pp. 1005–1011, Feb. 2014.

[101] P. Burasa, N. G. Constantin, and K. Wu, "High-data-rate single-chip battery-free active millimeter-wave identification tag in 65-nm CMOS technology," *IEEE Trans. Microw. Theory Techn.*, vol. 64, no. 7, pp. 2294–2303, Jun. 2016.

[102] T. C. Baum, R. W. Ziolkowski, K. Ghorbani, and K. J. Nicholson, "Embroidered active microwave composite preimpregnated electronics—Pregtronics," *IEEE Trans. Microw. Theory Techniq.*, vol. 64, no. 10, pp. 3175–3186, Sep. 2016.

[103] N. Chahat, M. Zhadobov, L. L. Coq, S. I. Alekseev, and R. Sauleau, "Characterization of the interactions between a 60-GHz antenna and the human body in an off-body scenario," *IEEE Trans. Antennas Propag.*, vol. 60 no. 12, pp. 5958–5965, Aug. 2012.

[104] Y. Cui, S. A. Nauroze, R. A. Bahr, and M. M. Tentzeris, "3D printed one-shot deployable flexible Kirigami dielectric reflectarray antenna for mm-Wave applications," in *Proc. IEEE MTT-S Int. Microw. Symp.*, 2020, pp. 249–258.

[105] T. S. Rappaport, F. Gutierrez, E. Ben-Dor, J. N. Murdock, Y. Qiao, and J. I. Tamir, "Broadband millimeter-wave propagation measurements and models using adaptive-beam antennas for outdoor urban cellular communications," *IEEE Trans. Antennas Propag.*, vol. 61 no. 4, pp. 1850–1859, Feb. 2013.

[106] Y. Zhang, "Antenna-in-package technology: Its early development [historical corner]," *IEEE Antennas Propag. Mag.*, vol. 61, no. 3, pp. 111–118, Jun. 2019.

[107] H. Zhang and A. Shamim, "Gain enhancement of millimeter-wave on-chip antenna through an additively manufactured functional package," *IEEE Trans. Antennas Propag.*, vol. 68 no. 6, pp. 4344–4353, Feb. 2020.

[108] H. Y. Kim, T. H. Jang, H. H. Bae, and C. S. Park, "A 60 GHz compact multidirectional-beam antenna-in-package for mobile devices," *IEEE Antennas Wireless Propag. Lett.*, vol. 18 no. 11, pp. 2434–2438, Sep. 2019.

[109] H. Gao, M. Matters-Kammerer, P. Harpe, and P. Baltus, "A 50–60 GHz mm-Wave rectifier with bulk voltage bias in 65-nm CMOS," *IEEE Microw. Wireless Compon. Lett.*, vol. 26, no. 8, pp. 631–633, Jul. 2016.

[110] J. G. D. Hester and M. M. Tentzeris, "Inkjet-printed flexible mm-Wave Van-Atta reflectarrays: A solution for ultralong-range dense multitag and multisensing chipless RFID implementations for IoT smart skins," *IEEE Trans. Microw. Theory Techn.*, vol. 64, no. 12, pp. 4763–4773, Nov. 2016.

[111] D. Henry, J. G. D. Hester, H. Aubert, P. Pons, and M. M. Tentzeris, "Long-range wireless interrogation of passive humidity sensors using Van-Atta cross-polarization effect and different beam scanning techniques," *IEEE Trans. Microw. Theory Techn.*, vol. 65 no. 12, pp. 5345–5354, Nov. 2017.

MAHMOUD WAGIH (Graduate Student Member, IEEE) received the B.Eng. degree (Hons.) from the University of Southampton in 2018, where he is currently pursuing the Ph.D. degree.

In 2017, he worked as a Research Assistant with the University of Southampton, investigating novel differential transmission lines. In 2018, he was a Hardware Engineering Intern with Arm, Cambridge, U.K., where he was a Research Intern in 2020. He has over 25 journal and conference publications and has delivered an invited webinar on these topics. His current research interests lie in RF energy harvesting, wireless power transfer, in addition to printed and wearable antennas.

Mr. Wagih was the recipient of the Best Undergraduate Project Prize at the University of Southampton in 2018, and was selected for the IEEE International Microwave Symposium Project Connect in 2019. He is the recipient of the Best Student Paper Award at the IEEE Wireless Power Transfer Conference in 2019 and the Best Oral Paper at PowerMEMS in 2019. He won the Best 3MT Presentation Prize (2^{nd} place) at the IEEE Microwave Week in 2020.

ALEX S. WEDDELL (Member, IEEE) received the M.Eng. (Hons.) and the Ph.D. degrees in electronic engineering from the University of Southampton, U.K., in 2005 and 2010, respectively.

He is currently a Lecturer with the Center for Internet of Things and Pervasive Systems, University of Southampton, and is involved with three projects funded by EPSRC, EU Horizon 2020, and Clean Sky 2. He has over 14 years' experience in design and deployment of energy harvesting systems, and has published around 55 peer-reviewed papers in the area. His main research focus is in the areas of energy harvesting and energy management for future Internet of Things devices.

STEVE BEEBY (Senior Member, IEEE) received the B.Eng. degree (Hons.) in mechanical engineering from the University of Portsmouth, Portsmouth, U.K., in 1992, and the Ph.D. degree in MEMS resonant sensors from the University of Southampton, Southampton, U.K., in 1998.

He is currently the Head of the Smart Electronic Materials and Systems Research Group, School of ECS, University of Southampton and leads the U.K.'s E-Textiles Network. He is currently leading three U.K. funded research projects and has received over 16 million research funding. He is a Co-Founder of Perpetuum Ltd., a University spin-out based upon vibration energy harvesting formed in 2004, Smart Fabric Inks Ltd., and D4 Technology Ltd. He has coauthored/edited four books, including *Energy Harvesting for Autonomous Systems* (Artech House, 2010). He has given 25 invited talks and has over 300 publications and ten patents. He has an h-Index of 52. His current research interests focus on energy harvesting, e-textiles, and the use of energy harvesting in wearable applications.

Dr. Beeby was the recipient of the two prestigious EPSRC Research Fellowships to investigate the combination of screen-printed active materials with micromachined structures and textiles for energy harvesting and was also awarded a Personal Chair in 2011. He is currently the Chair of the International Steering Committee for the PowerMEMS Conference series.